Design and Synthesis of Metal-Organic Framework Based Electrode Materials for Energy Storage

MSc Thesis

By SAFWANA SHIRIN KM



DEPARTMENT OF CHEMISTRY INDIAN INSTITUTE OF TECHNOLOGY INDORE MAY 2025

Design and Synthesis of Metal-Organic Framework Based Electrode Materials for Energy Storage

THESIS

Submitted in partial fulfillment of the requirements for the award of the degree of Master of Science

By SAFWANA SHIRIN KM



DEPARTMENT OF CHEMISTRY INDIAN INSTITUTE OF TECHNOLOGY INDORE MAY 2025



INDIAN INSTITUTE OF TECHNOLOGY INDORE

CANDIDATE'S DECLARATION

I hereby certify that the work which is being presented in the thesis entitled **Design and**Synthesis of Metal-Organic Framework-Based Electrode Materials for Energy Storage in the partial fulfilment of the requirements for the award of the degree of MASTER OF SCIENCE and submitted in the DEPARTMENT OF CHEMISTRY, Indian Institute of Technology Indore, is an authentic record of my own work carried out during the time period from July-2024 to May 2025 under the supervision of **Prof. Shaikh M. Mobin**

The matter presented in this thesis has not been submitted by me for the award of any other degree of this or any other institute.

21-5-2025

SAFWANA SHIRIN KM

Signature of the student with date

Satuana

This is to certify that the above statement made by the candidate is correct to the best of my/our knowledge.

May-21-2025

Prof. Shaikh M. Mobin

Signature of Supervisor with date

SAFWANA SHIRIN KM has successfully given her M.Sc. Oral Examination held on 14/5/2025.





ACKNOWLEDGEMENTS

I am deeply grateful to the Almighty for His guidance and for instilling in me the self-belief that has empowered me to pursue my dreams and become the person I am today. I also extend my sincere gratitude to myself for unwavering dedication and tireless efforts in turning those dreams into reality.

I would like to express my heartfelt appreciation to Prof. Shaikh M. Mobin for his invaluable supervision, motivation, and insightful suggestions. I am especially thankful to him for introducing me to the fascinating field of Metal-Organic Frameworks, which has significantly enriched my academic journey.

My sincere and enduring respect goes to Dr. Zahir Abbas, who has guided me throughout my research journey with immense patience and dedication.. His guidance from the very first day in the lab played a pivotal role in igniting my passion for research.

I am profoundly thankful to my beloved parents for their unconditional love, unwavering faith, and constant encouragement. Their support has been the cornerstone of my perseverance and success in completing this thesis. I also extend my heartfelt gratitude to Riswana Shirin and Farshan, who have always encouraged me to dream big and pursue my goals with confidence.

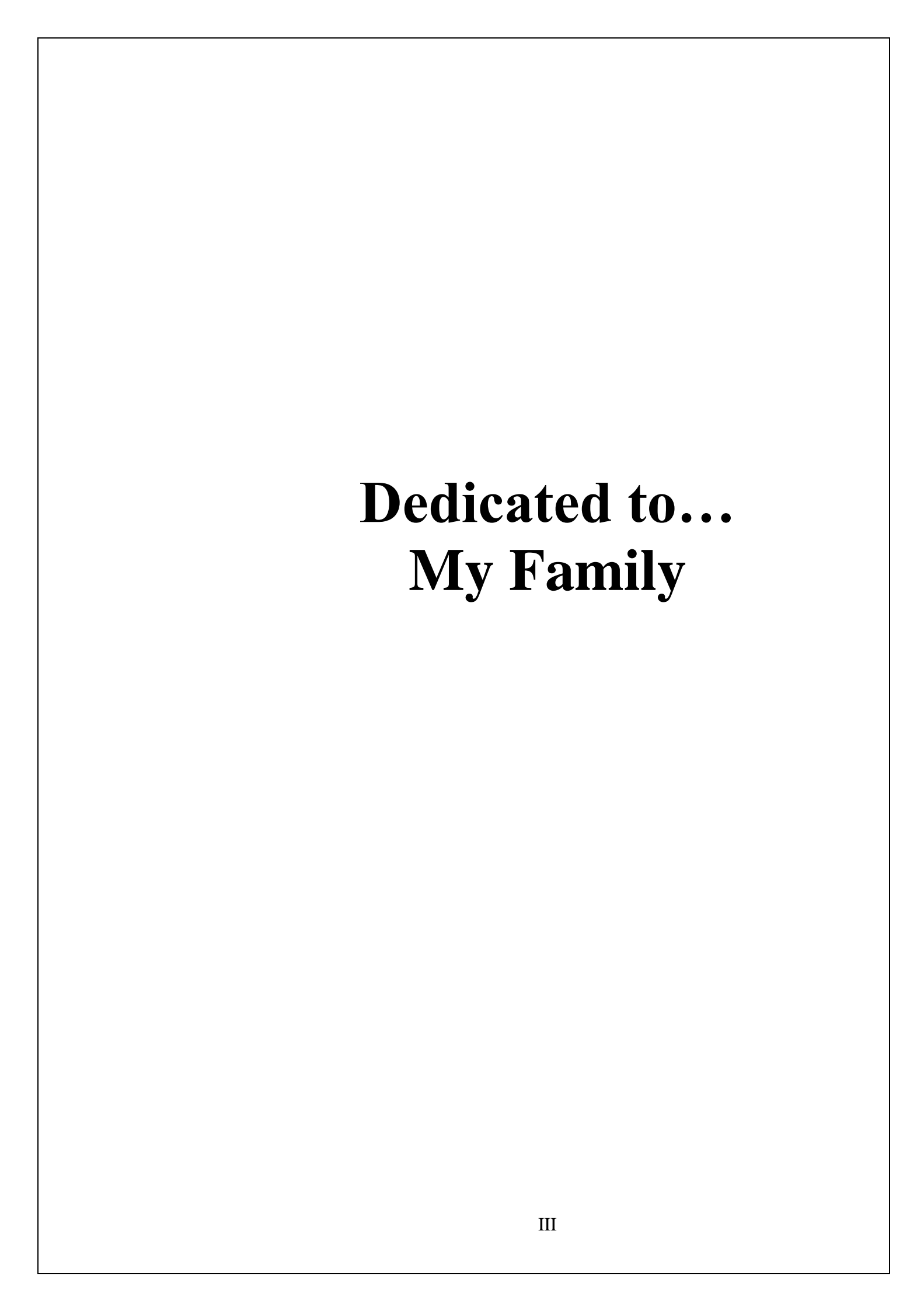
I am incredibly thankful to my dear friends Hiba and Ardra for their constant support and for always being there to listen and uplift me throughout this journey. A special thanks to Afrin and Tabinda for all the love and care you've given me, it meant so much. I'm also grateful to the wonderful people from 201 and to Shirin for the many meaningful conversations and quality time we shared.

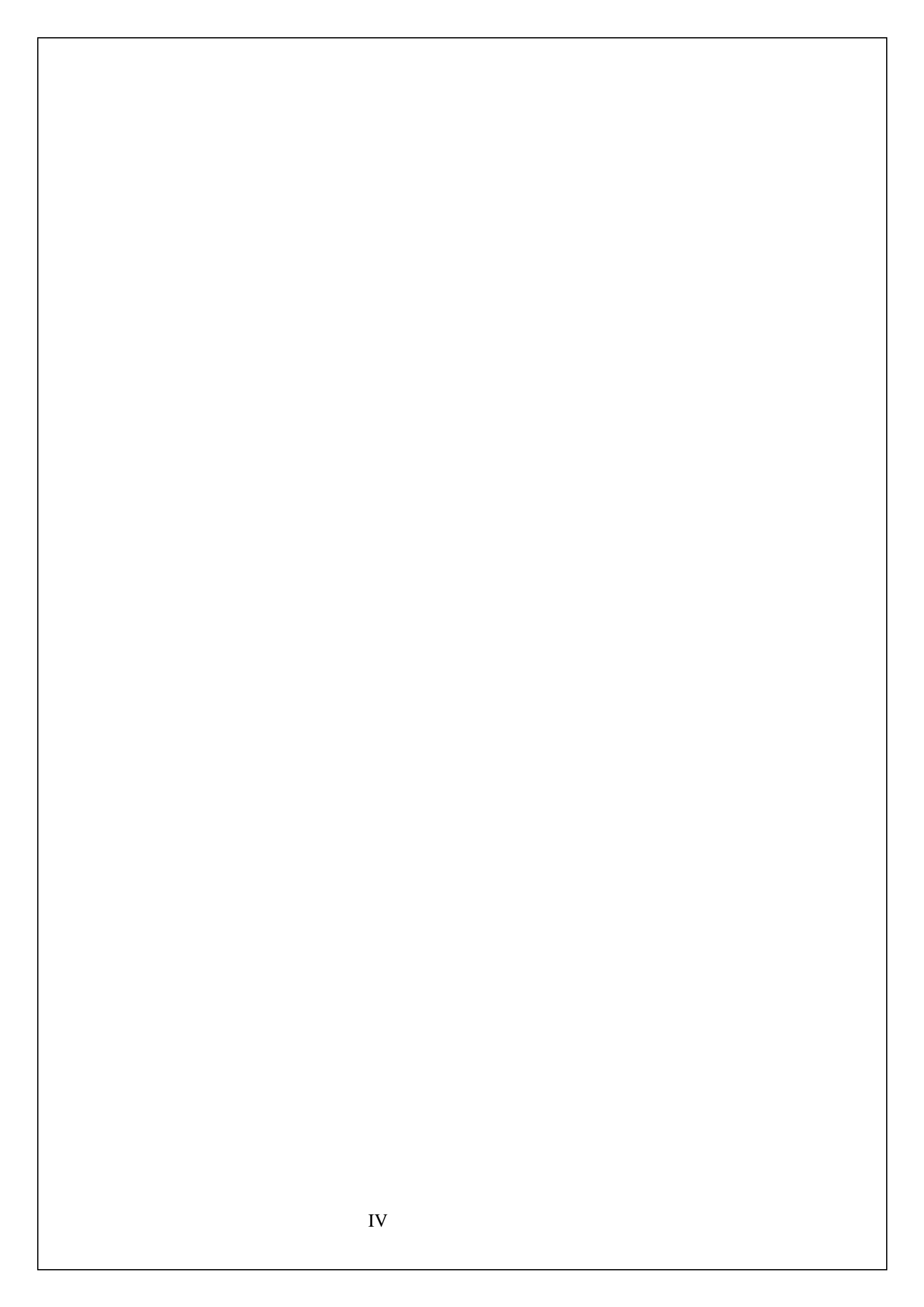
My sincere thanks to the Malayali Community for being a source of warmth, comfort, and belonging, through trips, shared meals, and joyful moments that brought a sense of home away from home.

Thank you to Khushi and SMM group lab mates, all of my batchmates MSc Chemistry-2023-25, SIC-IIT, for characterizations, and to each one of you who lent a helping hand, offered a kind smile, or took care of me

in any way. Your warmth and camaraderie have meant a great deal to me.

Finally, thank you to IIT Indore for this beautiful journey of learning and unlearning, for the wonderful experiences, life lessons, peaceful moments, and the best days of my student life. I am forever grateful for everything.





ABSTRACT

The development of supramolecular frameworks with tailored structural features remains challenging. Here, we report a novel cobalt-based functionalized layered framework (Co-MOF) synthesized via a mixedligand strategy using Azopyridine (AzPY) and 2,3,5,6-tetrafluoro-1,4benzenedicarboxylic acid (TF). The framework possesses unique structural advantages, including stable hydrogen bonding, π - π stacking, and a fluorinated functionalized network. Co-MOF features a Co(O₄N₂) coordination environment with two coordinated water molecules, contributing to an extended hydrogen-bonding network. Its electrochemical performance an electrode material for supercapacitors was evaluated. Electrochemical analysis reveals that Co-MOF exhibits a significantly higher specific capacitance of 956 F g⁻¹ at 1 A g⁻¹, along with an excellent cycling stability. Real-time device performance further confirms its enhanced energy density. These results highlight the potential of integrating electroactive building blocks with functionalized frameworks into real-world applications to achieve superior electrochemical properties. By precisely controlling ligand size, functional groups, and solvent-mediated synthesis, this strategy paves the way for the design of next-generation electrode materials for high-performance supercapacitors.

Keywords: Functionalized layered framework; H-bonding; π - π stacking; supercapacitor performance; ASC device.

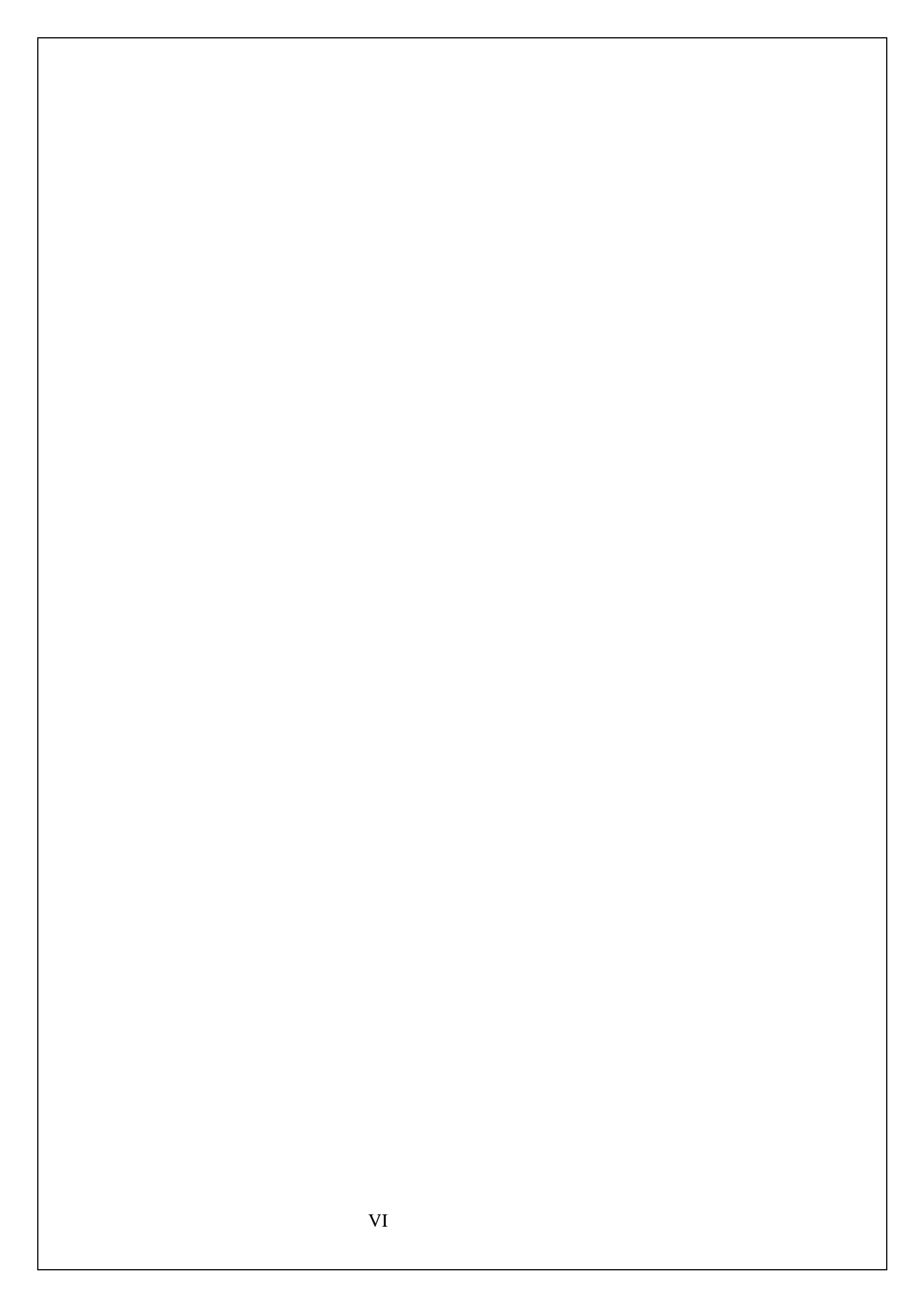


TABLE OF CONTENTS

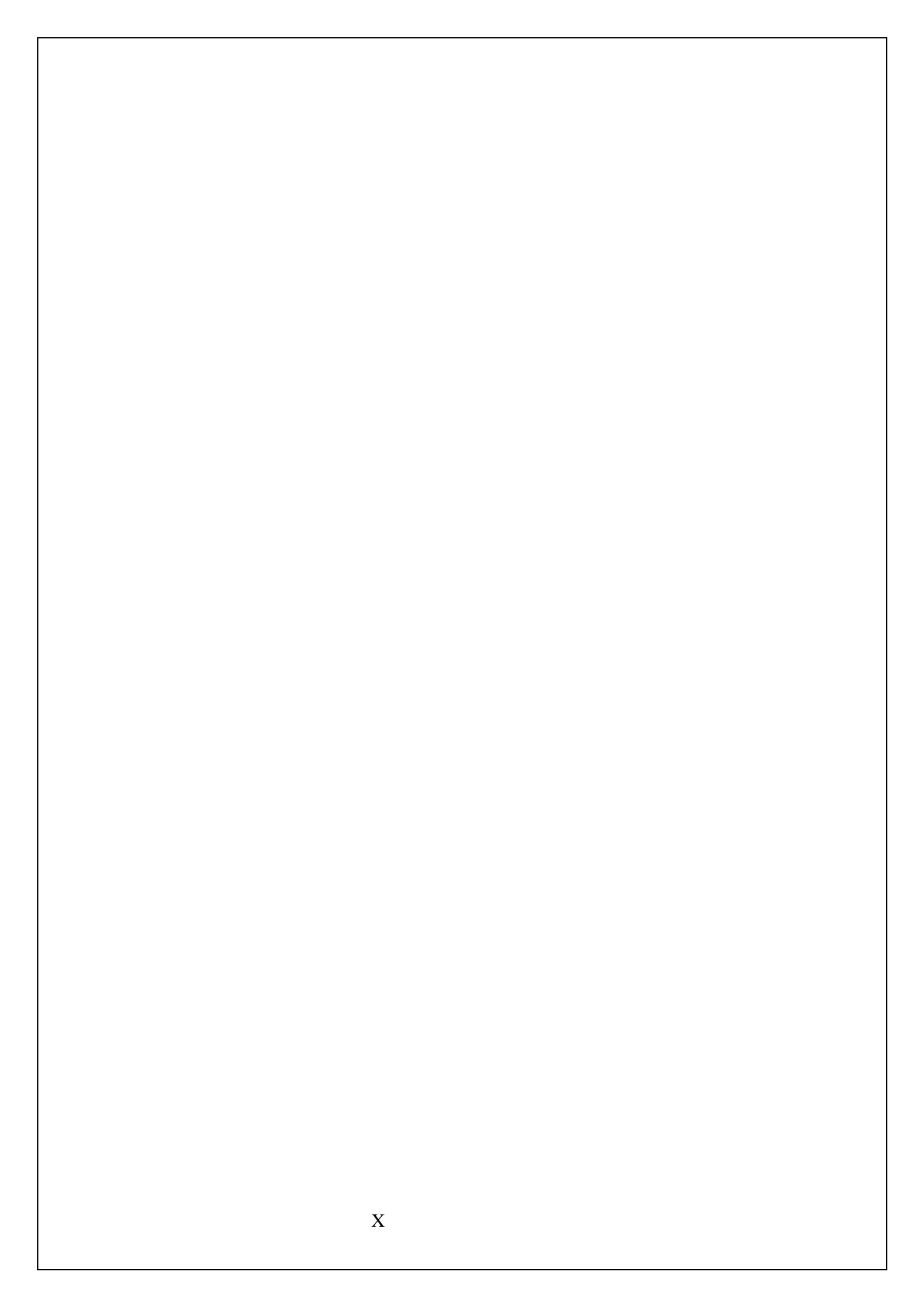
LIST OF SCHEMES	IX
LIST OF FIGURES	XI
LIST OF TABLES	X111
ABBREVIATIONS	XV
ACRONYMS	XVII
Chapter 1: INTRODUCTION	1-10
Metal-organic framework	
1.1 General Synthesis Protocol of MOFs	
1.2 Application of MOFs	
1.3.1 Metal-Organic Frameworks for Energy Ap	plications
Chapter 2: OBJECTIVES	11
Chapter 3: MOTIVATION	13
Chapter 4: LITERATURE SURVEY	15 -16
Chapter 5: EXPERIMENTAL SECTION	17-18
5.1 Materials	
5.2 Physical Measurements	
5.3 X-ray Crystallography Measurements	
5.4 Synthesis of Co-MOF	
Chapter 6: RESULTS AND DISCUSSION	NS 19-28
6.1 Structural description of (Co-MOF)	
6.2 XRD-Analysis	

6.4 FTIR	
6.5 TGA and BET	
6.6 XPS	
6.7 Electrochemical performance	
6.8. Device Performance	
Chapter 7: CONCLUSIONS	29
Chapter 8: SUPPORTING INFORMATION	31-41
8.1 Electrode Preparation and Electrochemical Measurement	
8.2 Efficiency Evaluation	
8.3 Device Fabrication	
Chapter 9: SCOPE OF WORK	43
Chapter 10: REFERENCES	45-54

6.3 SEM

LIST OF SCHEMES

Scheme 1. Schematic representation of the preparation 20 of Co-MOF



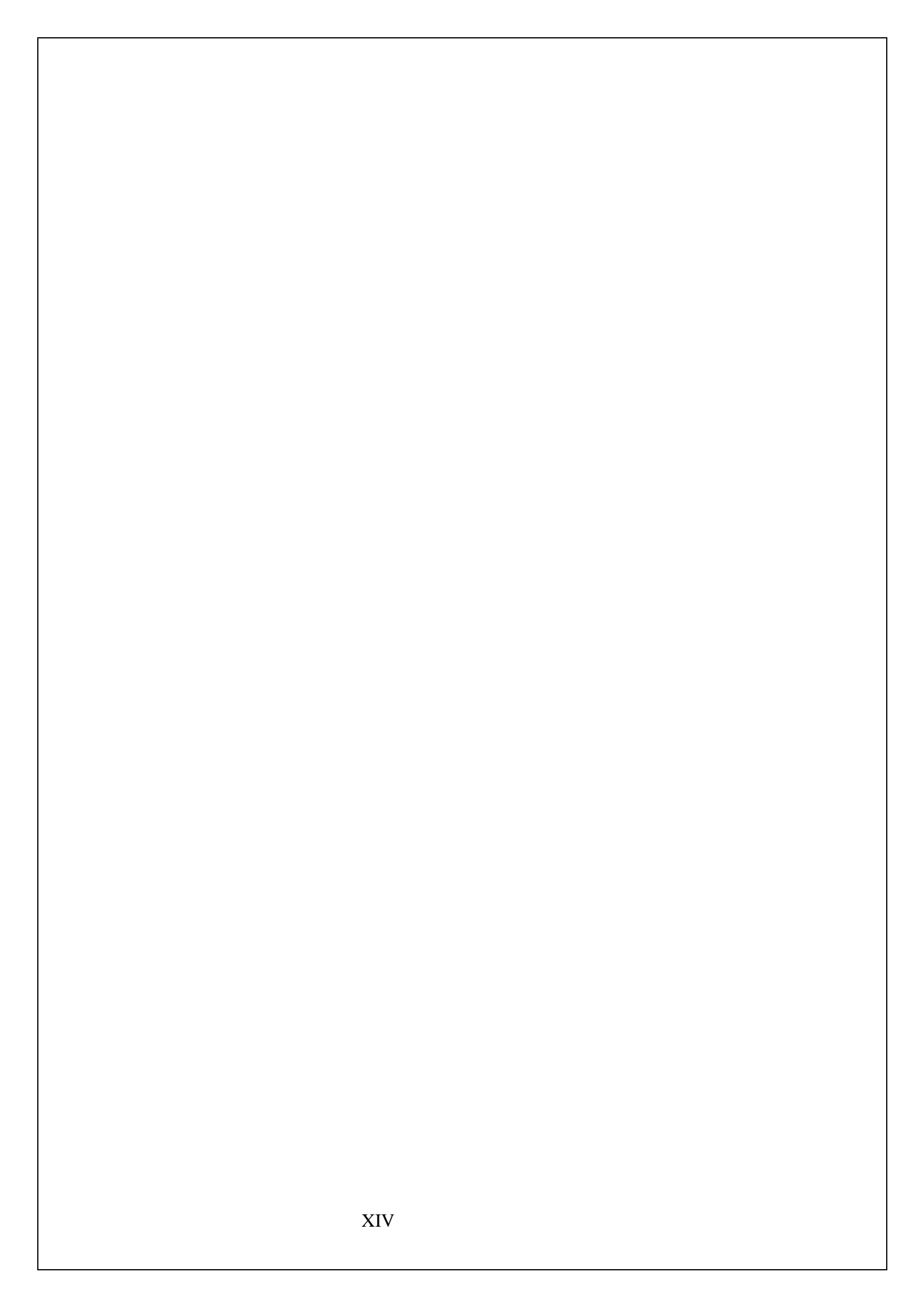
LIST OF FIGURES

Figure 1.11	Schematic representation of MOF	6
Figure 1.2	Organic linkers used in MOFs	7
Figure 1.3	Synthesis methods of MOF	8
Figure 1.4	Applications of MOF	11
Figure 2.1.	(a) Molecular binding mode (b) 2D layered	21
	network along c-axis (c) 2D view along	
	a-axis (d) Extended network via H-bonding	
	having π - π stacking in Co-MOF.	
Figure 2.2	a-b) As-synthesized and simulated PXRD of Co-	22
	MOF (c) SEM image of Co-MOF (d) XPS-Co 2p,	
	(e) XPS-F 1s, and (f) XPS-O 1s	
Figure 2.3	(b) Cyclic voltammetry of Co-MOF at different	24
	scan rates. (c) GCD of Co-MOF at different	
	current densities. (c) Bar Diagram-Specific	
	capacitance vs current density of Co-MOF (d)	
	Cyclic retention after 9000 GCD cycles (inset:	
	first 5 and last 5 cycles).	
Figure 2.4	(a) Schematic illustration of the ASC device. (b)	26
	Cyclic voltammetry of the ASC device at	
	different scan rates (c) GCD profile at different	
	current densities. (d) Bar diagram of specific	
	capacitance vs current densities. (e) energy	
	density vs power density plot (f) Cyclic retention	
	after 5000 GCD cycles (inset: first 5 and last 5	
	cycles)	
Figure 8.1	SCXRD data of Co-MOF (a) asymmetric unit (b)	31
	metal coordination geometry (c) Space filling	
	model.	
Figure 8.2	a) EDS Mapping of Co-MOF	31
Figure 8.3	(a) EDX elemental analysis Co-MOF	32
Figure 8.4	FT-IR spectra of Co-MOF	32
Figure 8.6	Thermogravimetric Profile of Co-MOF.	33

Figure 8.7	(a)BET adsorption-desorption isotherm of Co-	33
	MOF (b) BJH distribution of Co-MOF.	
Figure 8.8.	XPS spectra of Co-MOF (a) Survey Scan, (b) C	34
	1s and (c) N 1s.	
Figure 8.9	EIS plot of Co-MOF.	34

LIST OF TABLES

- Table 8.1X-ray crystal structure data and refinement 35parameters of Co-MOF.
- Table 8.2.Bond lengths and bond angles for Co-MOF36-38
- Table 8.3.SupercapacitorperformanceofCo-MOF39compared to other MOF-based materials.



ABBREVIATIONS

°C Degree Celsius

g Gram

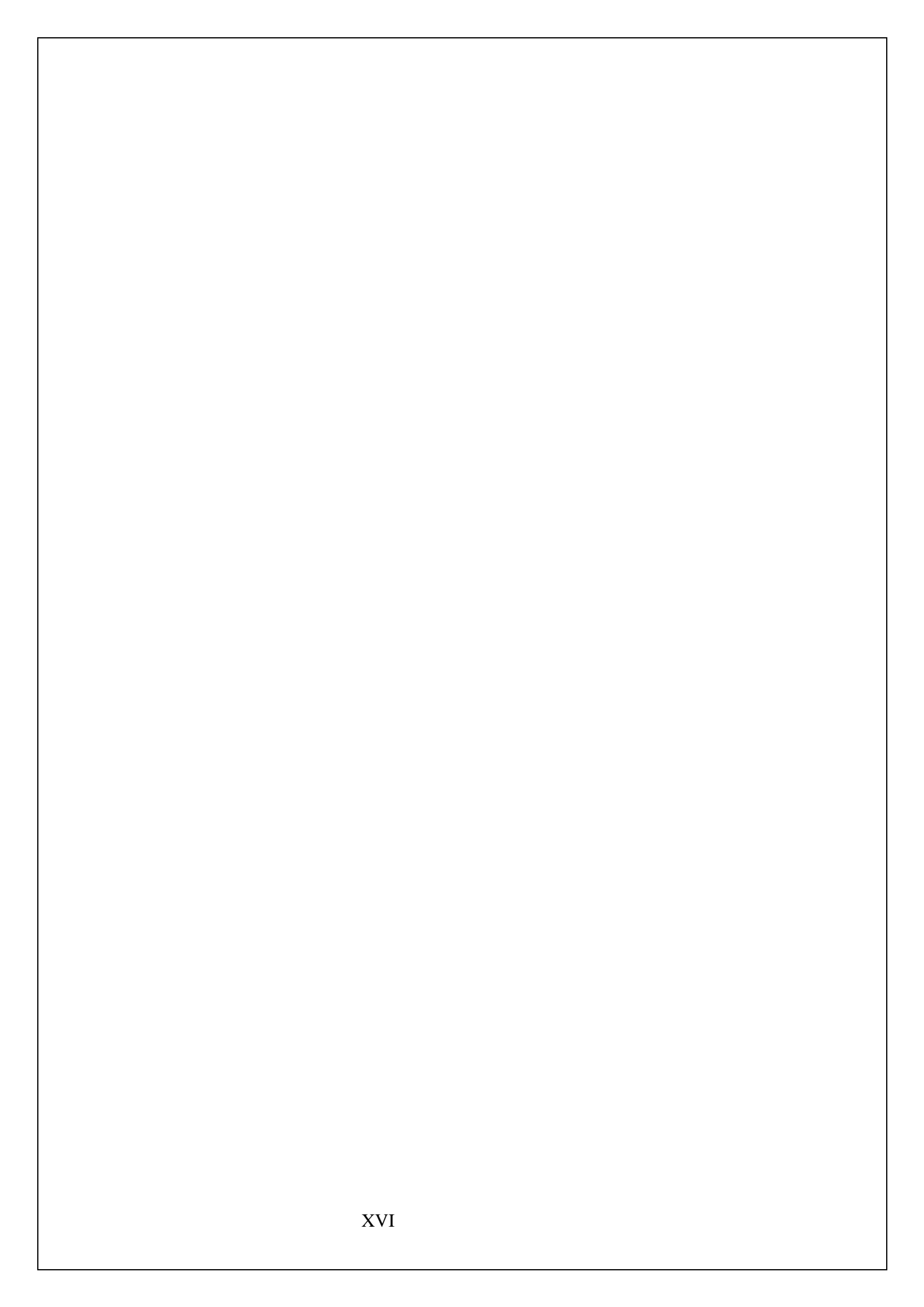
h Hour

mg Milligram

mL Millilitre

min Minutes

mol Mole



ACRONYMS

Abbreviations used here for substituents, reagents, etc. are largely in accordance with the recommendation of the IUPAC-IUC Commission on Biochemical Nomenclature, 1974, Pure and Applied Chemistry, 40, 315-331. Additional abbreviations used in this report are listed below.

AzPY Azopyridine

Dd Doublet of doublet

DMF Dimethyl acetamide

DMA Dimethylformamide

EtOA Ethyl acetate

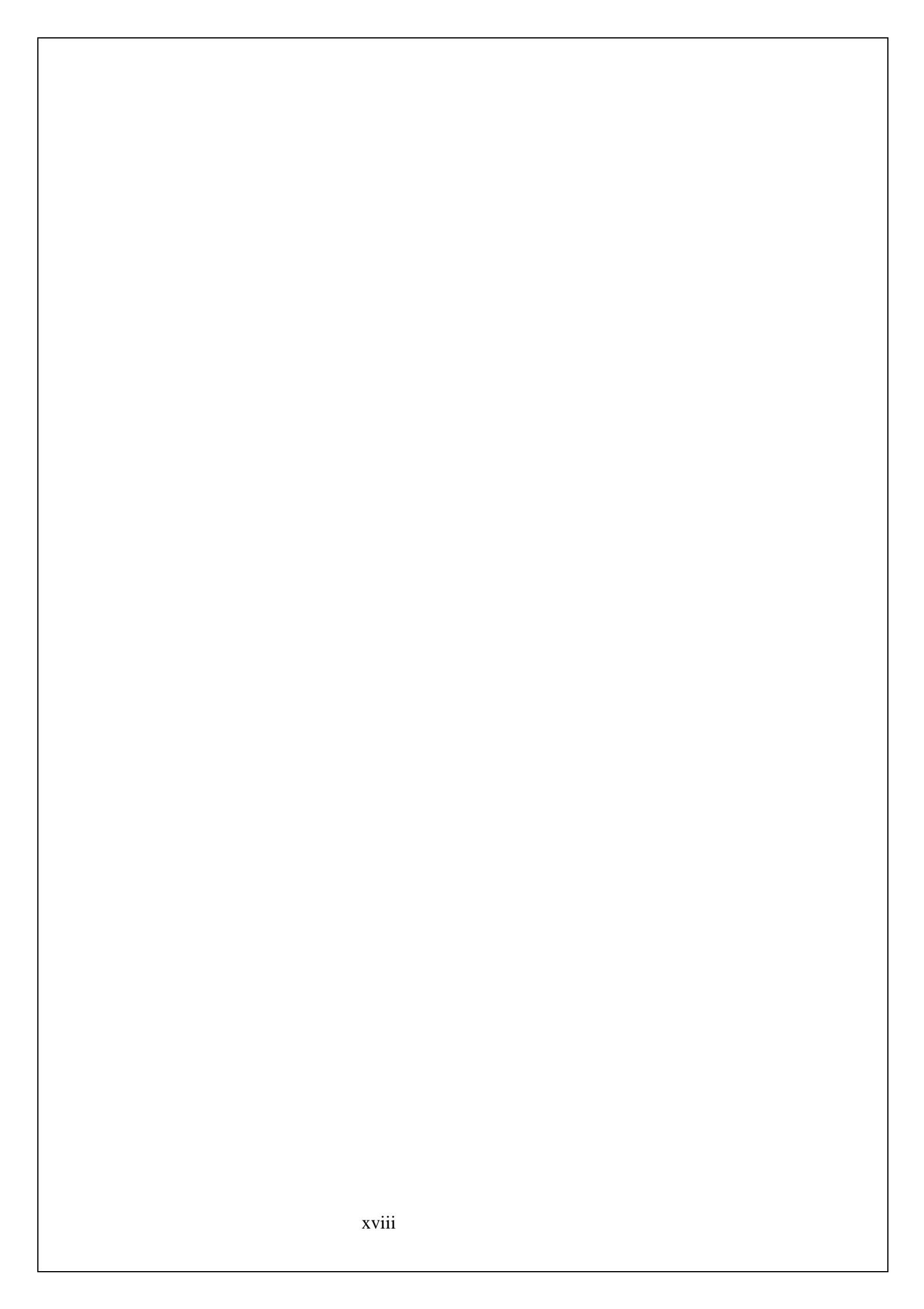
h Hour

MOF Metal-organic framework

mp Melting point

rt Room temperature

TF 2,3,5,6- tetrafluoro-1,4-benzenedicarboxylic acid



Chapter 1

INTRODUCTION

1.1 Metal-organic framework

Metal-organic frameworks (MOFs) are crystalline porous materials made up of organic and inorganic components. They are constructed from metal ions or clusters (called nodes or secondary building units, SBUs) that are coordinated to organic molecules called linkers. The linkers connect the metal centers in a highly ordered, cage-like structure with a very high internal surface area. MOFs differ from traditional porous materials with a complicated structure, tunable porosity, and various structures. While Zeolites are based on purely inorganic materials, MOFs have an easily tailored structure and chemistry of the framework, making them an attractive platform of materials that researchers can design and implement for various applications.² Research on MOFs has been relatively active for the last few decades, particularly because they may be directed to encapsulate guest molecules based on their size or shape. MOFs are highly versatile, and their tunable design can accommodate numerous functional groups, which would add additional properties and expand their literature applications.³

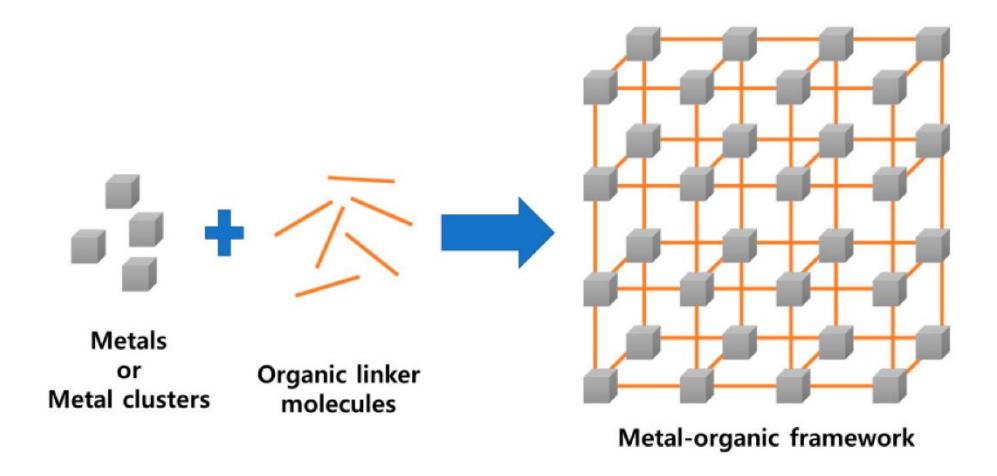


Figure 1.1: Schematic representation of MOFs.⁴

Compared to traditional microporous materials, MOFs have the advantage of design flexibility. MOFs are made from coordination bonds between metal atoms and an organic linker, which come together to form periodic porous crystalline materials. We call these porous coordination polymers (PCPs) depending on the metal center. The coordination chemistry alone has yielded thousands of unique MOF architectures. The porous nature of the MOFs also makes for a confined environment in which new chemical reactions and physical phenomena can take place.⁵ As a result, MOFs have become a popular focus in materials chemistry, also bridging chemistry, going into areas like cluster chemistry, organic synthesis, and crystallography. The applications of MOFs are vast and growing at a rapid pace. The fact that they can selectively catch certain molecules while allowing others to pass through is desirable for the separation process. Their high surface area allows for high-volume gas adsorption to increase storage options.⁶ In MOF, the organic linkers almost entirely based on carboxylic acids, are organophosphorus compounds, sulfonic acids, or heterocyclic molecules. The linkers can be linear, bent, or angular and influence the geometrical framework and pore structure. The reactivity and thermal stability of these linkers will also alter the surface area and thus the performance. Consequently, the geometry of a MOF is determined by both the spatial disposition of metal centres and the geometric parameters of the organic linkers.⁷

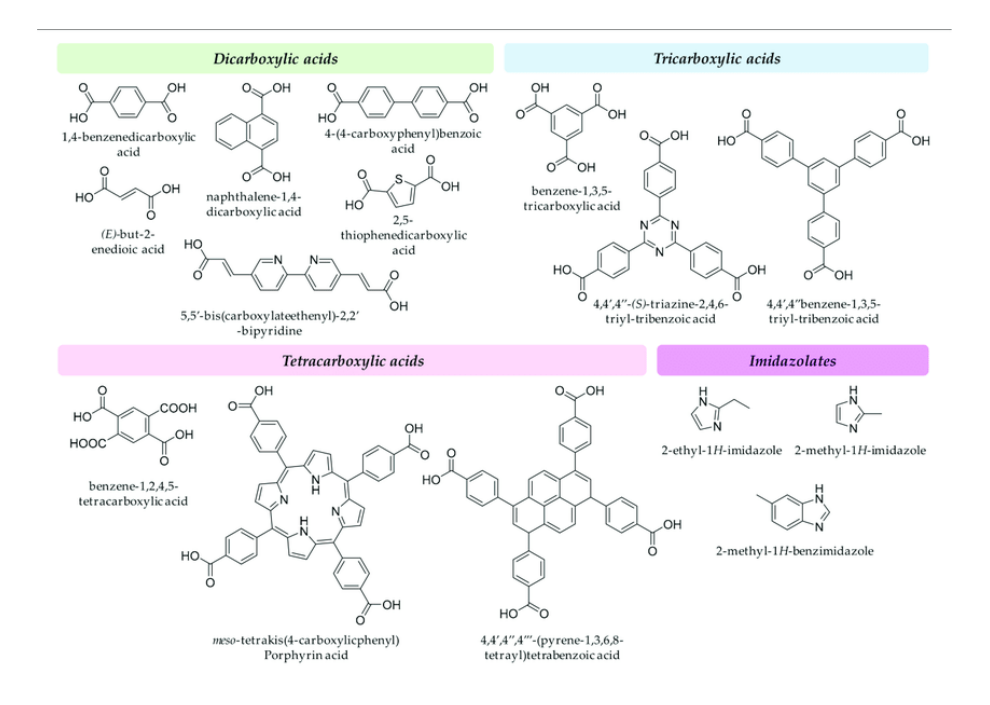


Figure 1.3Organic linkers used in MOFs.⁸

When it comes to MOFs, synthetic techniques mostly focus on the creation of metal-containing nodes and the coordination bonds that form between them. MOFs began with the goal of making inorganicorganic hybrid porous materials that acted like zeolites, in that they could employ the structural features of inorganic porous materials, while also being tunable by a wide range of organic moieties. In most early examples of MOFs, single-metal-ion nodes were more likely utilized, with the metal-based building units forming the nodes and the coordination bonds forming in situ through a one-pot synthesis.⁹ While organic linkers are most often pre-designed and chemically intact through the assembly process, the geometry of these ligands strongly determines the topology (and therefore also the possible diversity of structures) of the resultant MOF. By systematically varying metal-containing units and organic linkers, to form MOFs with particular functionalities, researchers created a practically limitless variety of MOFs - not just in structure but also in chemical properties and functionalities - for nearly every conceivable application.¹⁰

One difficulty associated with MOF synthesis is interpenetration, or the formation of multiple frameworks within large internal cavities, thereby reducing pore volume. This can be addressed by using linkers with the right size and geometry, for example. The size of the pores and the arrangement of cavities can be finely tuned by limiting the degrees of other properties of the metal centers and ligands, together with the reaction conditions. Also, the integration of MOF research with other fields of science has helped push the progress and development of this discipline, and allowed advanced materials for catalysis, gas storage, sensing and more.⁴

1.2 General Synthesis Protocol of MOFs

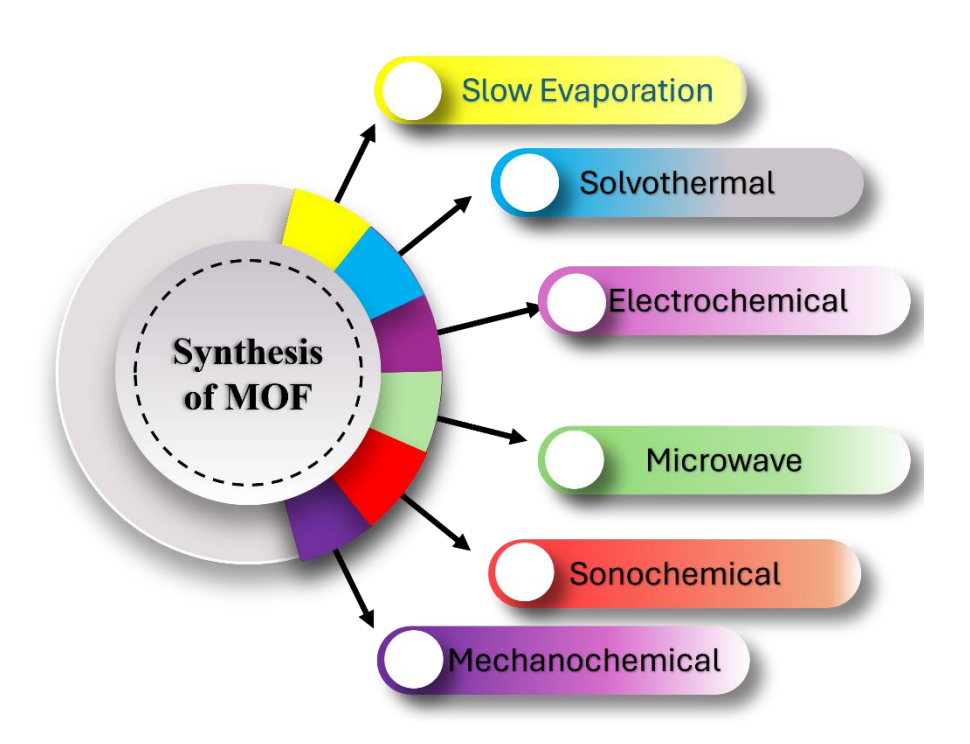


Figure 1.3: Synthesis methods of o MOF

1.2.1 Hydrothermal method

The hydrothermal method involves the self-assembly of products from soluble precursors. Initially used for synthesizing zeolites, this technique has also been adapted for the synthesis of metal-organic frameworks (MOFs). The process takes place in a sealed autoclave under autogenous pressure, with operational temperatures ranging from 80°C to 260°C. The cooling rate at the end of the reaction can significantly influence the outcome. However, these methods often require long reaction times, sometimes several days for solvothermal and hydrothermal techniques, and even weeks for the diffusion method.¹¹

1.2.2 Microwave method

Microwave-assisted MOF synthesis involves heating solutions with microwaves to form nanosized metal crystals. Although less common for crystalline MOFs, this rapid method allows precise particle shape and size control. Uniform seeding conditions are created, shortening the synthesis cycle. Suitable conditions include saturated solutions and temperature-dependent solubility, enabling crystal formation during cooling.¹²

1.2.3 Electrochemical method

The electrochemical method produces MOF powders industrially, offering advantages over solvothermal methods: no anions from metal salts, lower temperatures, and faster synthesis. In-situ metal ion generation near the support surface prevents unwanted crystal accumulation. Lower temperatures minimize thermal cracking during cooling. Electrochemical synthesis allows precise control via voltage adjustment or signal application (e.g., pulses), enabling finetuning.¹²

1.2.4 Mechanochemical synthesis

Mechanochemical synthesis uses mechanical force to initiate chemical reactions, avoiding solvents and reducing environmental impact. This method has been applied in various fields, including MOF synthesis, with benefits like:

- Ambient temperature reactions
- Short reaction times (10-16 minutes)
- Quantitative yields
- Water as the only byproduct (when using metal oxides)
- Structure-directing properties with liquid-assisted grinding (LAG) and ion- and liquid-assisted grinding (ILAG).¹³

1.2.5 Sonochemistry Method

Sonochemistry uses high-energy ultrasound (20 kHz - 10 MHz) to initiate chemical reactions. Cavitation creates microjets, dispersing particles and activating surfaces. Reactions occur in cavities, interfaces, or bulk media, leading to radical formation, bond breakage, and excited molecules. Sonochemistry enhances dissolution and is widely used in organic and nanomaterial synthesis. In MOF science, Sono chemical synthesis aims to be quick, eco-friendly, energy-efficient, and easy to use at ambient temperatures. Rapid reactions make it suitable for scaling up MOF production.¹⁴

1.3 Application of MOFs

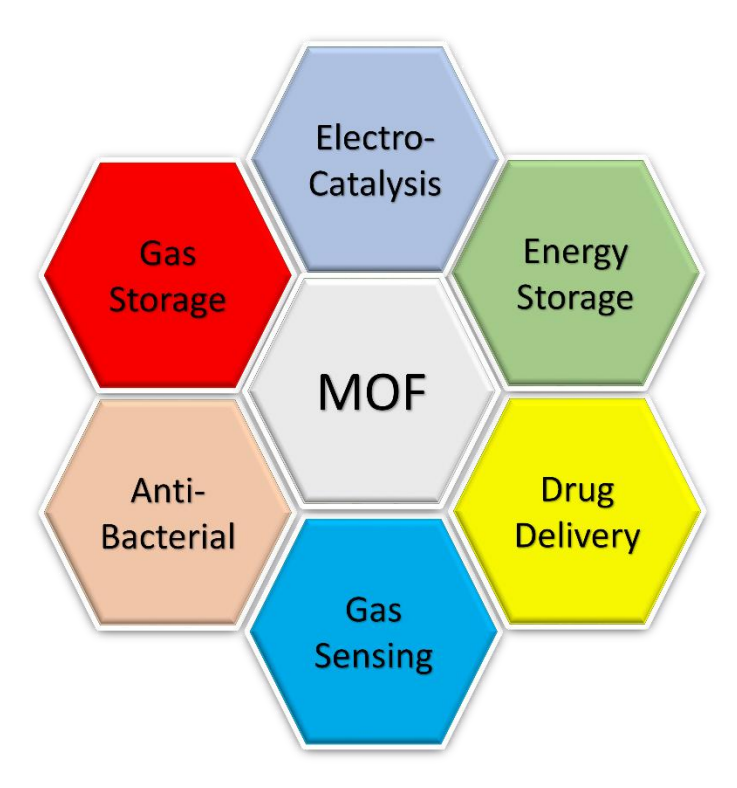


Figure 1.4: Applications of MOF

Metal-organic frameworks (MOFs) have a wide range of applications, including:

- ➤ Gas storage and separation: MOFs are used for gas storage and separation, and their pore structure can be adjusted to achieve this.
- Adsorption: MOFs are used in adsorption, a technique that's used to remove contaminants from water.
- ➤ Drug delivery: MOFs are used as carriers for drug delivery, allowing them to carry active compounds through the body.
- ➤ Biosensing: MOFs are used in biosensing for molecular detection, protein analysis, and cell imaging.
- ➤ Energy storage and conversion: MOFs have applications in energy storage and conversion.
- ➤ Catalysis: MOFs are used as catalysts in industrial processes.
- ➤ Wastewater treatment: MOFs are used in wastewater treatment, especially for removing dyes. Hydrogen storage: MOFs can store hydrogen because of their large surface area.

MOFs are versatile and tunable materials, and their applications are expanding rapidly. They are used in a wide range of fields, including chemistry, electronics, biomedicine, and more.¹⁵

1.3.1 Metal-Organic Frameworks for Energy Applications

The need for energy storage has intensified due to the depletion of fossil fuels and climate change concerns. Renewable energy sources require efficient storage solutions to address intermittency. Traditional batteries have limitations in energy density, charge/discharge rates, and lifespan. Supercapacitors offer a promising alternative, storing energy through charge separation on electrode surfaces. They excel in high-energy storage, rapid charge/discharge cycles, and prolonged lifespan, making them ideal for applications where batteries fall short. Supercapacitors (SCs), as a promising energy storage solution, have attracted considerable interest for their high power capability, exceptional safety, and reliable cycling stability.

To enhance eco-friendly energy conversion and storage technologies, developing highly efficient and durable catalysts and electrode materials with optimal electrochemical and photochemical properties is crucial. Tailoring compositions and nanostructures can introduce multifunctionality, increase surface area, and reduce charge carrier transport distances. This rational design approach enables:

- Enhanced active site accessibility
- Suppressed electron-hole recombination
- Improved kinetics

MOFs have garnered significant research interest for energy storage in supercapacitors because of their exceptional properties, including:

- ❖ High surface area: MOFs have extremely high surface areas, allowing for efficient storage of energy carriers like hydrogen and carbon dioxide.
- Pore size: MOFs pore sizes can be tailored to suit specific energy storage applications, enabling selective adsorption and desorption of energy carriers.

- High thermal stability: MOFs exhibit excellent thermal stability, making them suitable for high-temperature energy storage applications.
- Chemical stability: MOFs are resistant to chemical degradation, ensuring long-term performance in energy storage applications.
- ❖ Flexibility: MOFs can be designed to store various energy carriers, including gases, liquids, and ions.
- Scalability: MOFs can be synthesized in large quantities, making them suitable for industrial-scale energy storage applications.
- ❖ Low cost: MOFs can be synthesized from abundant and inexpensive materials, reducing production costs.
- Environmental friendliness: MOFs are non-toxic and noncorrosive, making them an environmentally friendly option for energy storage.

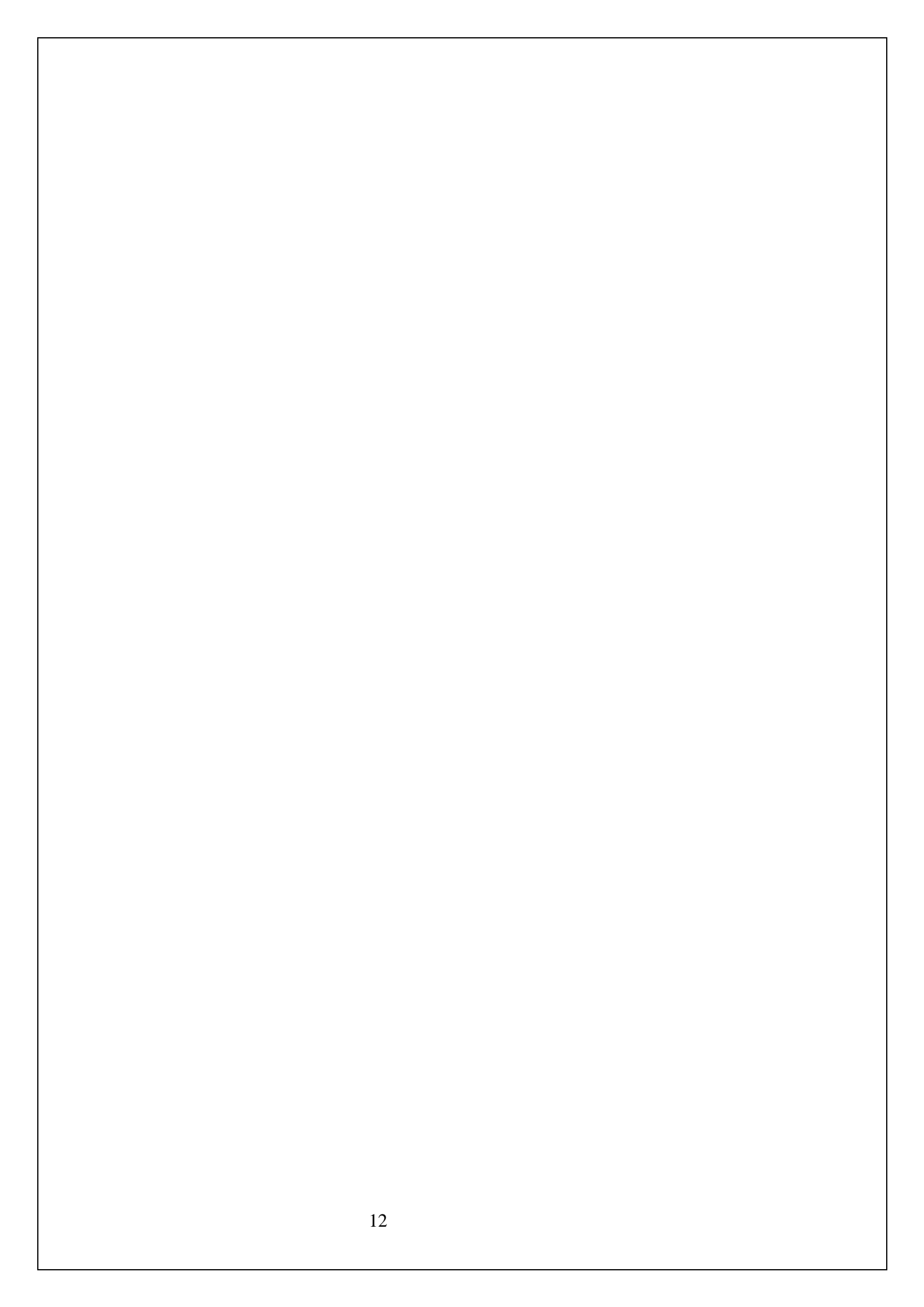
As one of the most important energy storage devices, SCs with both high-power densities and energy densities can bridge the gap between conventional capacitors and rechargeable batteries. Specifically, hybrid SCs normally constructed with capacitor-type electrodes and batterytype Faradaic electrodes, and asymmetric supercapacitors constructed with capacitor-type and pseudocapacitive electrodes have attracted much attention due to the high-power densities and energy densities. SCs are commonly recognized as an up-and-coming energy storage technology for the forthcoming generation. The primary factors contributing to their rapid charging/discharging capabilities and longer cycling life are well-documented in many sources. MOFs possess conductivity and show great potential in various fields, particularly in supercapacitors (SCs). The conductivity in the MOFs arises mainly from pathways that enable ion or electron transport between the inorganic components and the framework's structure. 18 Applications of this span multiple fields, including energy storage. In recent years, significant

advancements have been				
Frameworks (MOFs) for dire	ect use as super	capacitor elect	rodes	

Chapter 2

OBJECTIVES

- Synthesis of a functionalized Metal-organic framework (MOF).
- Development of MOF-based electrode materials for energy storage applications
- To extensively characterize material properties of the synthesized metal-organic framework using various techniques like Single crystal XRD, Powder XRD, SEM, FESEM, TEM, FTIR, BET, and TGA
- To investigate the electrochemical properties of the synthesized metal-organic framework
- To fabricate the device for practical applicability.
- To understand and explore the workings of many instruments.

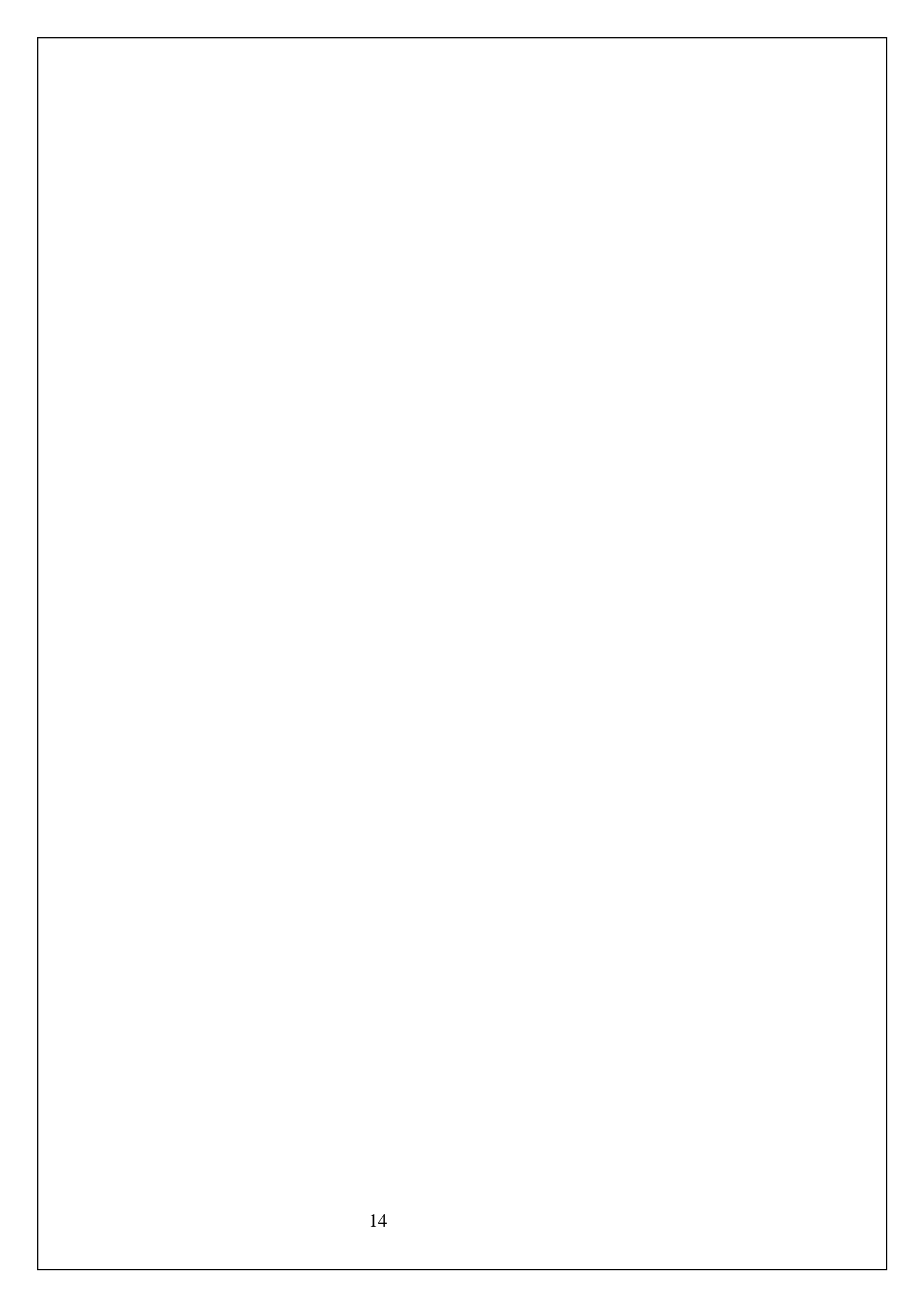


MOTIVATION

The world faces an unprecedented energy crisis, with escalating global demands and an urgent need to transition to alternative energy sources. Efficient energy storage solutions have become critical to addressing this challenge. Traditional energy storage systems often struggle to meet the growing demand. Electrochemical storage solutions, like batteries and supercapacitors, are pivotal in addressing this critical need. Characterized by their high surface area and tunable porosity, MOFs offer a promising solution for enhancing energy storage capacities.¹⁹

By focusing on MOF-based materials, we aim to develop systems that can store energy more effectively and sustainably, addressing one of the most pressing challenges of our time. MOFs possess a unique combination of properties, including tunable pore sizes and diverse chemical functionalities. This versatility allows for the customization of electrode materials to optimize performance based on specific applications, such as batteries and supercapacitors. For instance, the ability to manipulate the structural parameters of MOFs can lead to enhancements in ion transport and conductivity, critical factors for efficient energy storage.²⁰ Exploring this adaptability is crucial for advancing energy storage technologies. Despite the promise of MOFs, significant gaps remain in understanding their interactions and performance as electrode materials. The complex relationships between MOF structures and their electrochemical properties require thorough investigation. Addressing these gaps not only contributes to the fundamental understanding of material science but also paves the way for innovative applications in energy storage.²¹

We aim to design and synthesise an affordable, highperformance functionalised MOF and develop Metal-Organic Framework-based electrode materials for supercapacitor applications. This involves creating and synthesizing novel MOF structures with optimized characteristics.



LITERATURE SURVEY

Specifically designed advanced materials offer a great advantage to renewable energy with significant potential to reduce environmental carbon emissions by eliminating greenhouse gases and pollutants. As global energy demands rise and technology advances, efficient energy storage systems have become indispensable. Batteries and supercapacitors represent pivotal technologies for energy storage. However, the inherent limitations of batteries have redirected significant research focus towards supercapacitor materials. Supercapacitors are ideal for applications requiring fast energy delivery and durability. These attributes position supercapacitors as a critical area of research, with the synthesis of unique structural features and materials, and stability of high-performance electrode materials playing a key role in advancing innovative and sustainable energy storage solutions for future smart energy devices. 27,28

Metal-organic frameworks (MOFs) are a distinctive class of crystalline materials formed by linking organic molecules with metal ions, resulting in highly ordered frameworks with exceptional versatility. 29,30 The layered framework is a subclass of 2D MOFs that possesses structural features suitable for energy applications, including a sheet-like layered structure, abundant active sites, a large surface area, and is extended via stable hydrogen bonding (H-bonding) and π - π stacking. 31 In addition to stacking, the strong in-plane covalent bonds support electron delocalization within ultra-thin two-dimensional structures, improving their electrochemical performance and making them highly suitable for electrical device applications. These layered frameworks can be functionalized to achieve specific properties. 32

Functionalization is an effective strategy for improving the properties of electrode materials.. ^{33,34} Halogen-functionalized electrode materials have demonstrated significant potential in enhancing the performance of energy storage devices, especially in supercapacitors (SCs). ³⁵ The synergistic properties of halogen-functionalized materials help in

22enhancing the efficiency of supercapacitors. These strategies are well documented in the literature, but most of the studies were explored via heteroatom-doped functionalization strategies. Zhu et al. reported the synthesis of an F, N co-doped porous carbon nanosheet (F/N-CNS), which exhibited fast reaction kinetics and enhanced pseudocapacitive properties.³⁶ Similarly, ZIF-67 was utilized as a precursor to develop N, F dual-doped hierarchical nanoporous carbon polyhedron (NFHPC), which, as a negative electrode material achieved an impressive specific capacitance of 305 F g⁻¹ at a current density of 1 A g⁻¹.³⁷ A comprehensive investigation into this area is crucial to unlocking new opportunities for optimizing energy storage systems and addressing the growing demand for high-performance, sustainable energy solutions.³⁸ Fluorine (F), as the most electronegative element (4.0) among halogens and other non-metals, causes a significant concentration of electron density on polarized C-F bonds, which imparts superior properties to fluorine-functionalized electrode materials. Compounds having abundant semi-ionic C-F bonds demonstrate enhanced electronic conductivity and an increased number of active sites, making them highly efficient as electrode materials.^{35,39}

Inspired by the idea of functionalization, we designed a fluorinated cobalt framework, having desirable structural features such as extension of the layered framework via H-bonding and π - π stacking. This novel electrode material for supercapacitors was synthesized via a slowdiffusion method at room temperature (RT) by using a mixed-ligand strategy, where TF (2,3,5,6-tetrafluoro-1,4-benzenedicarboxylic acid) and AzPY (4,4'-azopyridine) are used as ligands. Functionalization improves the electrochemical properties of layered frameworks, and the H-bonded network provides stability, while the mixed-ligand approach incorporating carboxyl-rich and nitrogen-donor linkers further enhances their performance. 40 Additionally, the crystal structure of cobalt-based layered frameworks shows greater tunability and superior physicochemical properties compared to other systems.

EXPERIMENTAL SECTION

5.1 Materials:

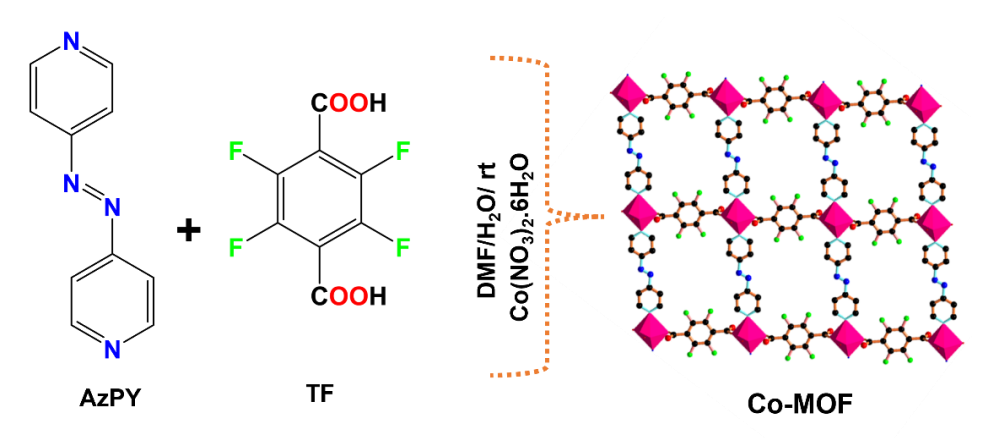
2,3,5,6-tetrafluoro-1,4-benzenedicarboxylic acid (TF) and Azopyridine (AzPY) were obtained from Sigma-Aldrich. Co(NO₃)₂·6H₂O, and N, N-dimethylformamide were procured from Merck and SRL Chemicals and used without further purification. Deionized water (DI) was used to prepare electrolytes.

5.2 Physical Measurements: Single-crystal analysis was conducted at low temperatures using a CCD-equipped SuperNova diffractometer. Powder X-ray diffraction (PXRD) was performed with Cu Kα radiation (λ = 1.5406 Å) on a Rigaku SmartLab X-ray diffractometer. The FT-IR spectrum, ranging from 4000 to 400 cm⁻¹, was recorded using a Bio-Rad FTS 3000MX instrument with KBr pellets. Thermogravimetric analysis (TGA) was carried out on a METTLER TOLEDO TGA/DSC1 system, employing STARe software at a heating rate of 10 °C min-1 under a nitrogen atmosphere up to 800 °C. Morphological studies were performed using a Supra55 Zeiss field emission scanning electron microscope (FESEM). The BET surface area and pore size distribution were measured using an Autosorb iQ system, version 1.11 (Quantachrome Instruments). X-ray photoelectron spectroscopy (XPS) analyses were conducted with a Thermo Scientific MULTILAB 2000 instrument.⁴¹

5.3 X-ray Crystallography Measurements: Single-crystal X-ray diffraction (SCXRD) data was obtained using a Rigaku Oxford SuperNova CCD diffractometer at 293 K, employing monochromatic graphite Mo K α radiation ($\lambda = 0.71073$ Å). Data acquisition was managed with the CrysAlisPro CCD software, while essential reductions and refinements were carried out using CrysAlisPro RED. The crystal structure was determined using direct methods and further refined with SHELXL-97 by least-squares fitting based on F¹. All non-hydrogen atoms were refined anisotropically, while hydrogen atoms

were placed geometrically and refined with isotropic displacement parameters, typically set at 1.2Ueq of their parent atoms.⁴²

5.4. Synthesis of Co-MOF



Scheme 1. Schematic representation of the preparation of Co-MOF **Synthesis of Co-MOF**

Co-MOF was synthesized via a slow diffusion-based crystallization method by dissolving Azopyridine (0.05 mmol) in dimethylformamide (2 mL) and 2,3,5,6-tetrafluoro-1,4-benzenedicarboxylic acid (0.05 mmol) in DI water (2 mL). These 2 ligand solutions were mixed, and the resulting mixture was stirred for 30 min to form a clear solution. The aqueous solution of (0.1 mmol, 30 mg) Co(NO₃)₂·6H₂O (1 mL) was added to the ligand solution. After adding metal, this solution was kept for 6 days, and reddish crystals were observed to form. The crystals were isolated and washed with DMF to ensure high purity.

RESULTS AND DISCUSSION

A novel Cobalt-Functionalized Layered Framework (Co-MOF) was synthesized based on a mixed-ligand strategy by utilizing Azopyridine (AzPY) and 2,3,5,6-tetrafluoro-1,4-benzenedicarboxylic acid (TF) as ligands and Co(NO₃)₂.6H₂O as metal salt, via slow diffusion-based crystallization at room temperature, as depicted in **Scheme 1**. The obtained single crystal of Co-MOF was authenticated with single-crystal X-ray diffraction (SC-XRD) analysis. It confirms structural properties, functionalization, H-bonding, and π - π stacking. Furthermore, morphology, functional group, and structural properties were analysed via powder-XRD, SEM, ATR-FTIR, TGA, and XPS studies. Promising results prompted us to further evaluate its performance in energy storage.

6.1 Structural description of (Co-MOF)

The crystalline architecture of Co-MOF was elucidated through singlediffraction (SCXRD) crystal X-ray analysis, confirming its crystallization in a triclinic lattice system under the space group P-1. Detailed crystallographic parameters are presented in **Table 8.1.** The asymmetric unit of Co-MOF consists of one Co (II) ion, half of 2,3,5,6tetrafluoro-1,4-benzenedicarboxylic acid (TF), half of the Azopyridine (AzPY) moiety, as well as two coordinated water molecules (Figure **8.1a**). The molecular unit consisting of Co (II) is coordinated into two oxygen atoms of two TF molecules (both are coordinated in a monodentate fashion), two N atoms of AzPY linker, and two oxygen atoms of the coordinated water molecules (Figure 2.1a). This leads to the formation of an O₄N₂ environment around the Co (II) metal center, resulting in a distorted octahedral geometry (Figure 8.1b). The measured bond distance for the Co-O bond ranges from 2.124 Å to 2.141Å. Each AzPY is linked to two Co (II) centers with the measured bond distance of Co-N being 2.218 Å. The resulting TF and AzPY linkers relate to Co (II), showing a finite 2D framework along the c-axis as depicted in **Figure 1b**. The 2D view along the a-axis is shown in **Figure 1c**.

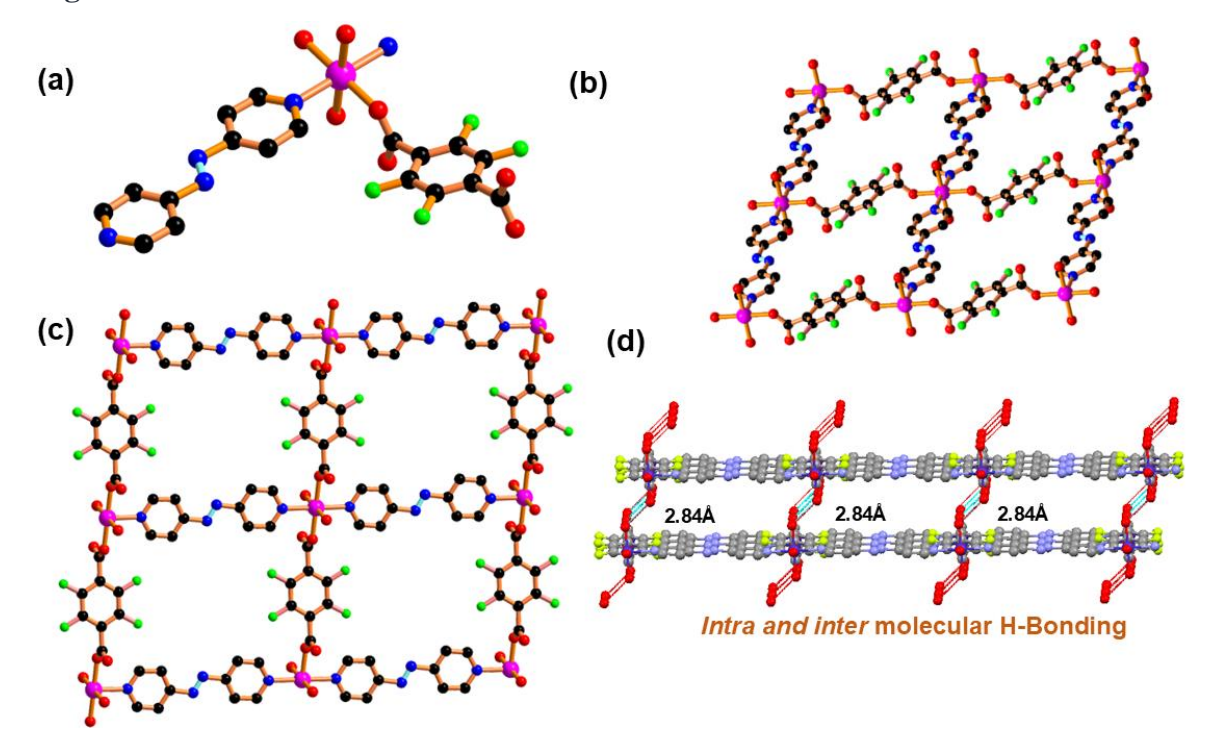


Figure 2.1. (a) Molecular binding mode (b) 2D layered network along c-axis (c) 2D view along a-axis (d) Extended network via H-bonding having π - π stacking in Co-MOF.

The H-bond, extended network with intra- and intermolecular H-bonding with the distance of 2.789 and 2.883 Å, respectively, is shown in **Figure 2.1d**. The layer-by-layer extension of the network with π - π stacking leads to improved strength and stability for the network and, thereby to better electrochemical performance. The space-filling model showing the porous network is given in **Figure 8.1c**. The significant bond lengths (Å) and bond angles (degrees) are summarised in **Table 8.2**.

6.2. XRD-Analysis

Powder X-ray diffraction analysis (PXRD) profiles of the synthesized Co-MOF exhibited a good correspondence with the simulated diffraction patterns derived from SC-XRD data, as illustrated in **Figure 2.2(a-b)**.

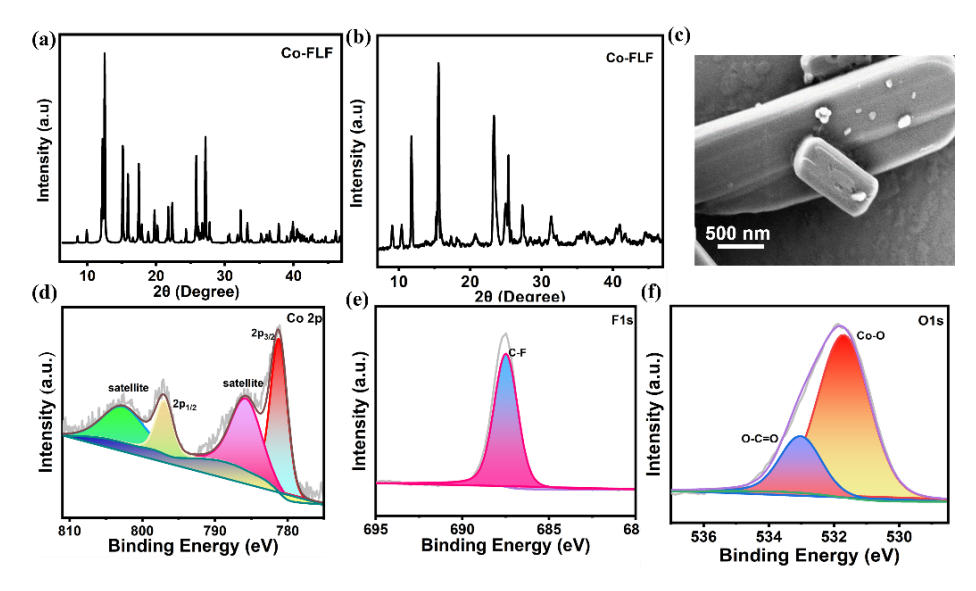


Figure 2.2. (a-b) PXRD patterns of Co-MOF (c), SEM image of Co-MOF (d), XPS Co 2p (e), XPS-F 1s, and (f) XPS-O 1s.

6.3. SEM

Morphological analysis was carried out by employing scanning electron microscopy (SEM). For Co-MOF, it shows Rod-like structures as recorded at different magnifications, 500 nm and 200 nm, shown in **Figure 2.2(c)**. EDX elemental analysis confirms the presence of all the expected elements, such as C, N, O, F, and Co, which is well aligned with the data from the SC-XRD analysis, emphasizing the material's homogeneous composition and structural consistency (**Figure 8.2**). EDS mapping confirms the presence of elements indicating their distribution within the analysed region (**Figure 8.3**).

6.4. FTIR

Attenuated Total Reflectance - Fourier Transform Infrared (ATR-FTIR) analysis was used to determine the bonding nature of Co-MOF. The bands in the 1508–1672 cm⁻¹ region correspond to the asymmetric stretching vibrations of carboxylate groups⁴³, while the 1411 cm⁻¹ band is attributed to the -N=N- moiety from the AzPY ligand.⁴⁰ Additionally, bands in the 400–600 cm⁻¹ region, assigned to Co-O and Co-N stretching vibrations, confirm the successful incorporation of cobalt into the framework structure through its interaction with oxygen or nitrogen donor atoms from the organic linkers. The presence of bands

at 1395 cm⁻¹ (symmetric C-F stretching) and 988 cm⁻ (asymmetric C-F stretching) shows their presence in Co-MOF, confirming the successful functionalization of fluorine in the Co-MOF structure (**Figure 8.4**)

6.5. TGA and BET

Thermogravimetric analysis (TGA) was conducted to evaluate the thermal structural stability of Co-MOF over a Temperature range of 50–800 °C and under a nitrogen atmosphere at a heating rate of 10 °C/min. The TGA profile reveals a minimal initial weight loss between 35 °C and 198 °C, attributed to the elimination of water molecules. The results in **Figure 8.5** demonstrated that Co-MOF possesses excellent thermal stability up to 350 °C. Subsequent weight loss is observed, corresponding to the decomposition of the organic framework structure. To determine the surface area and permanent porosity, Co-MOF was evaluated through N₂ adsorption-desorption analysis performed at 77 K. The Brunauer-Emmett-Teller (BET) surface area was determined to be 23.3 m² g⁻¹, while the Barrett-Joyner-Halenda (BJH) pore size distribution indicated an average pore diameter of 1.69 nm. (**Figure 8.6**).

6.6. XPS

X-ray Photoelectron Spectroscopy (XPS) was utilized to elucidate the elemental composition, functionalization, and oxidation state of Co-MOF. The survey scan spectrum of Co-MOF (Figure 8.9(a)) confirms the presence of Co, F, O, N, and C elements in Co-MOF. The highresolution deconvoluted XPS spectrum of Co 2p (Figure 2.2(d)) shows distinct peaks at 781.28 eV and 796.95 eV, attributed to the $2p_{3/2}$ and 2p_{1/2}, respectively. Notably, two satellite peaks emerged at 803.4 eV and 784.7 eV, corresponding to the Co $2p_{1/2}$ and Co $2p_{3/2}$ transitions. ^{44,45} The F 1s spectrum shows a peak at 687.48 eV, confirming the presence of the C-F bond in Co-MOF (Figure 2.2(e))⁴⁶ and thus successful functionalization in the framework structure. The O 1s spectrum displays two distinct signals at 533.08 eV and 531.68 eV, corresponding to the O-C=O and Co-O bonding environments, respectively (Figure 2(f)). 47,48 The C 1s spectrum is deconvoluted into four discrete peaks at binding energies of 284.8 eV, 285.96 eV, 286.08 and 287.28 eV, which are attributed to C-C, C-O, C-N, and C-F bonds, respectively (Figure **8.9(b)**). ^{49,50} The N 1s spectrum exhibited three distinct peaks at 398.6 eV, 399.80 eV, and 401.5 eV, which are assigned to Co-N bonds, pyridine nitrogen, and the azo group of AzPY, respectively (**Figure 8.9(c)**). ⁵¹ The XPS results further support the FTIR and confirm the formation of the C–F bond, indicating successful functionalization. This and the desirable structural stability advantages, such as H-bonding and π - π stacking identified through different characterization methods, encouraged us to evaluate the electrochemical performance of Co-MOF in supercapacitors.

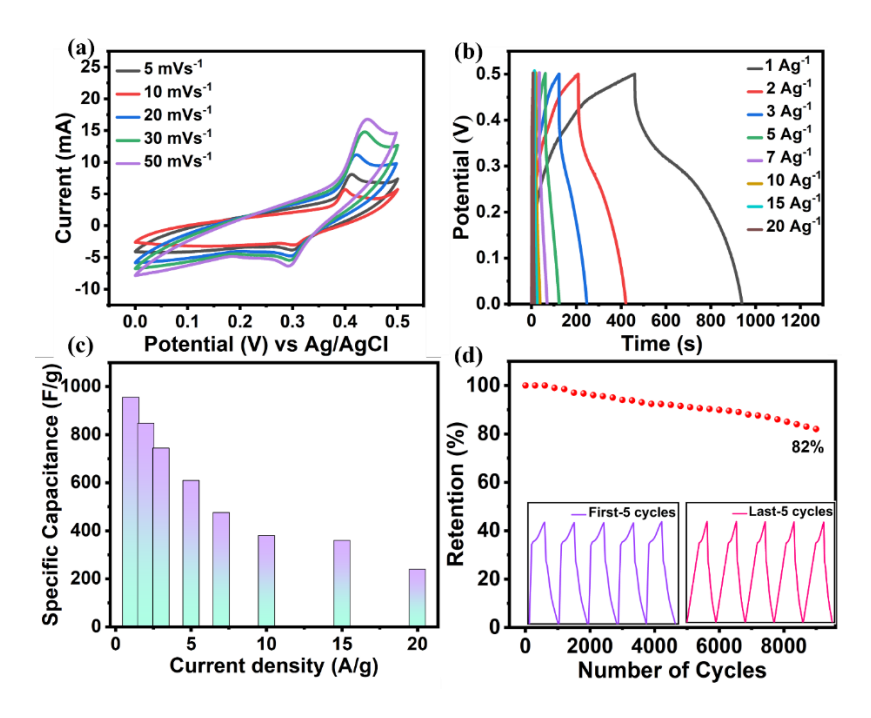


Figure 2.3. (a) Cyclic voltammetry of Co-MOF at different scan rates. (b) GCD of Co-MOF at different current densities. (c) Bar Diagram-Specific capacitance vs current density of Co-MOF (d) Cyclic retention after 9000 GCD cycles (inset: first 5 and last 5 cycles).

6.7. Electrochemical Performance

Co-MOF served as the electrode active materials in three and twoelectrode configurations by employing a 2 M KOH aqueous electrolyte to evaluate the electrochemical performance for supercapacitor applications. CV profiles of Co-MOF were recorded at different scan rates (5, 10, 20, 30, and 50 mV/s). The results indicate a proportional increase in the area enclosed by the CV curves with increasing scan rates while maintaining their original shape. This signifies excellent rate capability and robust electrochemical stability of the electrode material (Figure 2.3(a)). CV curves reveal that the material demonstrates pseudocapacitive characteristics, as seen from the presence of two well-defined redox peaks. These peaks arise from interactions at the electrode-electrolyte interface, driven by the intercalation and deintercalation of OH- ions during the faradaic redox process. Notably, the oxidation peak shifts toward a more positive potential, while the reduction peak shifts toward a more negative potential. This behaviour suggests that the electrode material enhances the irreversible tendencies of the electrochemical reaction, a phenomenon attributed to electrode polarization. From the galvanostatic charge-discharge profile (Figure 2.3(b)) of Co-MOF assessed at various current densities between 1 to 20 A g⁻¹, Co-MOF demonstrated remarkable specific capacitances of 956, 848, 744, 609.6, 476, 360, and 240 F g^{-1} under varying current densities of 1, 2, 3, 5, 7, 10, 15, and 20 A g^{-1} respectively.

The high specific capacitance value of Co-MOF is attributable to the layered framework of the compound and the functionalization of fluorine 52 . Layered framework materials serve as ideal electrode materials due to their well-structured internal crystal arrangement. 53,54 The structure also contributes to the performance of supercapacitors. In the Co-MOF structure, there is stacking due to the presence of van der Waals forces, π - π stacking, hydrogen bonding interactions, and the strong repulsive force of C-F bonds, which enlarges the interlayer space within the Co-MOF. By increasing the electronegativity of the functionalized atom, specific capacitance also increases. Fluorine is the most electronegative element, and it enhances the capacitance by acting as the site for effective charge accumulation and improves electrochemical behaviour by enhancing the transport of charges. This phenomenon suggests that the strong electronegativity of halogen atoms facilitates electron/ion transport and diffusion, significantly aiding the

charge storage process. Previous reports suggest that N- or F-doped (or functionalized) materials exhibit rapid kinetics and enhanced pseudocapacitive properties. These modifications improve ion transport, making them more efficient for energy storage applications. In contrast, conventional electrode materials often suffer from sluggish ion-transfer kinetics, which limits their overall performance.⁵⁵ All the abovementioned factors contribute to Co-MOF exhibiting better specific capacitance.⁵⁶

The variation of specific capacitance at different current densities for Co-MOF is illustrated in Figure 2.3(c), which shows that there is a decrease in specific capacitance with an increase in current densities, attributed to the fast charge transport occurring at higher current densities.⁵⁷ For practical applicability, it is vital to investigate the longterm cyclic stability of the electrode material. We measured cycling retention for 9000 GCD cycles at 15 A g⁻¹, which showed a cyclic retention of 82% as shown in Figure 2.3(d). The inset of the figure shows the first five and last five GCD cycles. To determine the charge transfer kinetics and internal resistance of the electrode materials via electrochemical impedance spectroscopy (EIS), measurements were made on a Nyquist plot to analyse the charge transfer kinetics at the electrode/electrolyte interface. These measurements were performed over a frequency range of 0.1 Hz to 100 kHz in a 2M KOH electrolyte to evaluate the kinetic behaviour of the electrode material. Co-MOF exhibits a lower charge transfer (R_{ct}) value of 2.58 Ω (**Figure 8.10**). This confirms the better electrical conductivity and higher electrochemical performance. These advantages of the electrode material prompted us further to evaluate its performance in real-time applications.

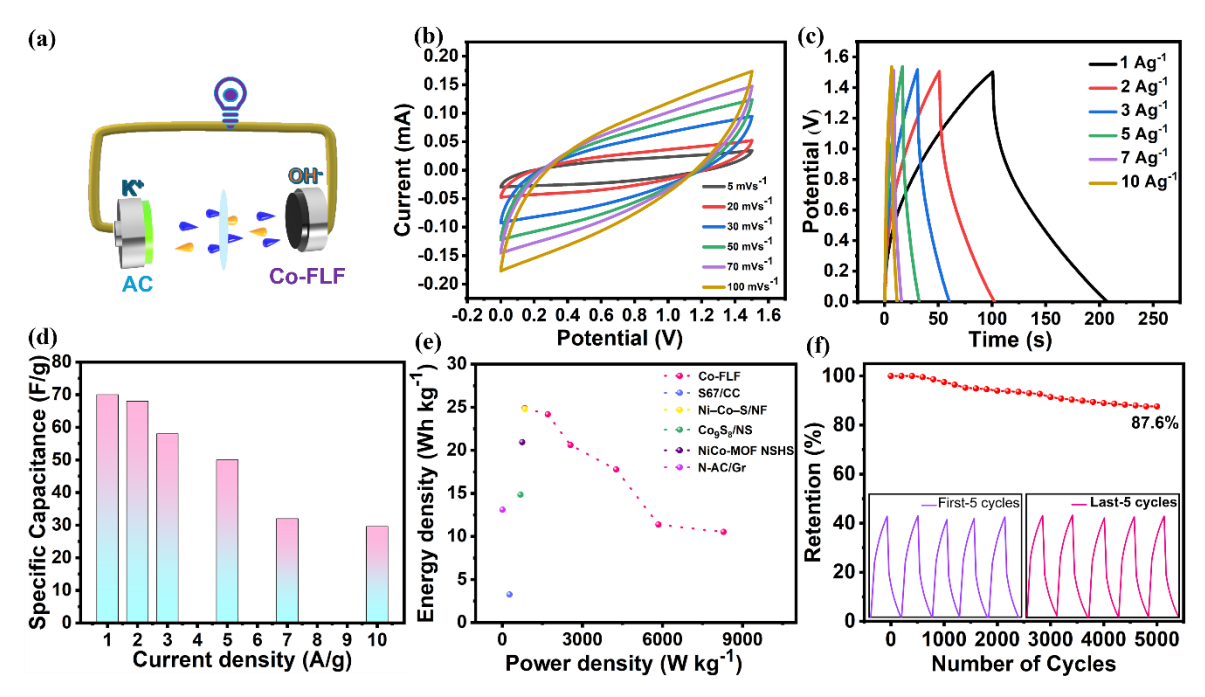


Figure 2.4. (a) Schematic illustration of the ASC device. (b) Cyclic voltammetry of the ASC device at different scan rates (c) GCD profile at different current densities. (d) Bar diagram of specific capacitance vs current densities. (e) Energy density vs power density plot (f) Cyclic retention after 5000 GCD cycles (inset: first 5 and last 5 cycles).

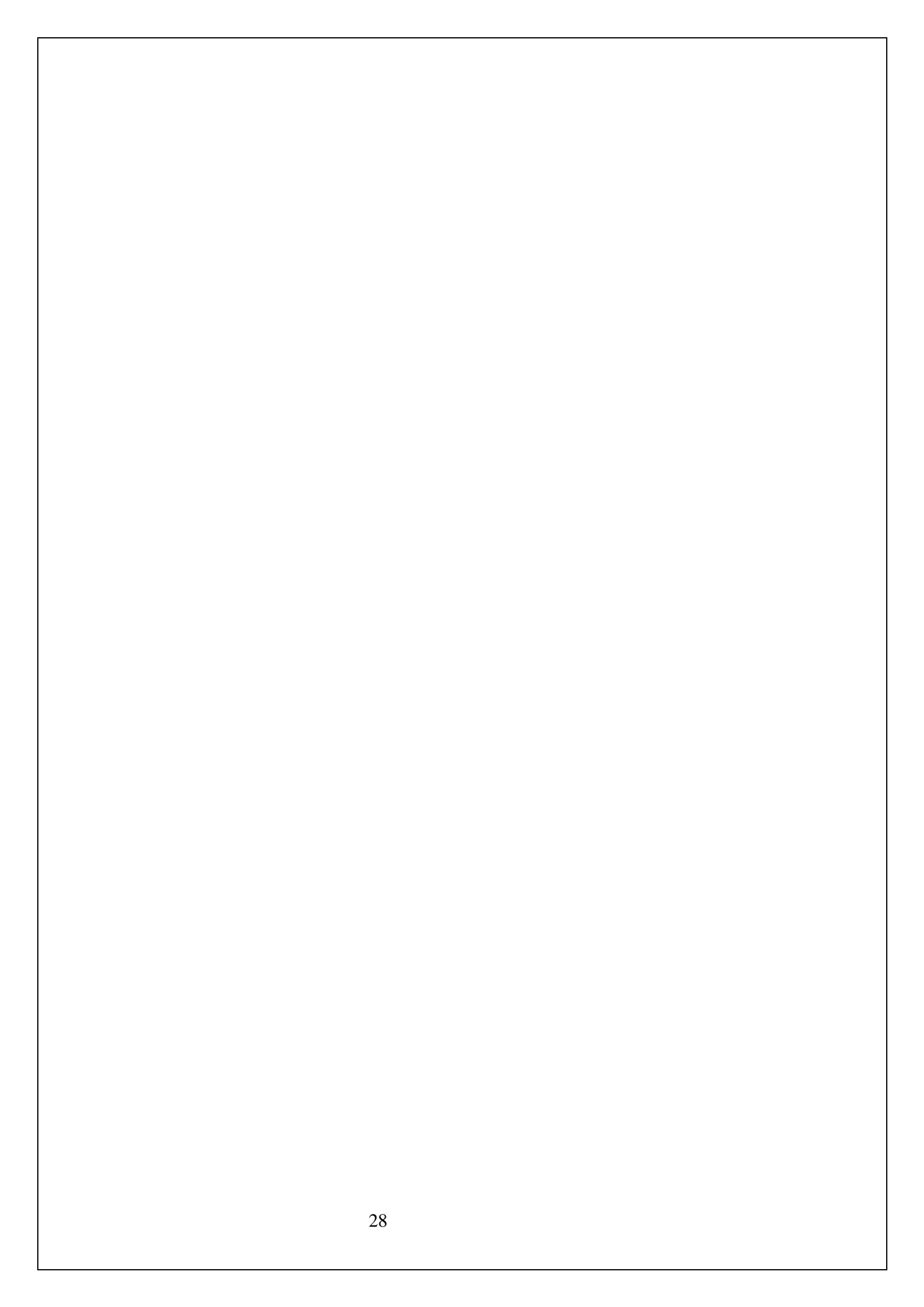
6.8. Device Performance

Driven by the superior electrochemical performance shown, the practical applicability of Co-MOF was evaluated using a two-electrode system. This approach aimed to assess its potential for real-world energy storage applications. The asymmetric supercapacitor (ASC) device was fabricated using Co-MOF as the positive electrode and carbon black as the negative electrode, with cellulose paper serving as the separator and PVA-KOH utilized as electrolyte. The complete ASC device configuration is illustrated in **Figure 2.4(a)**. To demonstrate its practical applicability, the device was charged using a 300 mAh AC adapter, and it powered a 1.8 V LED bulb for several seconds.

Cyclic voltammetry (CV) measurements of the Co-MOF ASC device were performed at various scan rates (5, 20, 30, 50, 70, and 100 mV/s) in the working potential range of 0-1.6 V. The CV curves exhibited no significant variation in shape at the different scan rates, indicating good

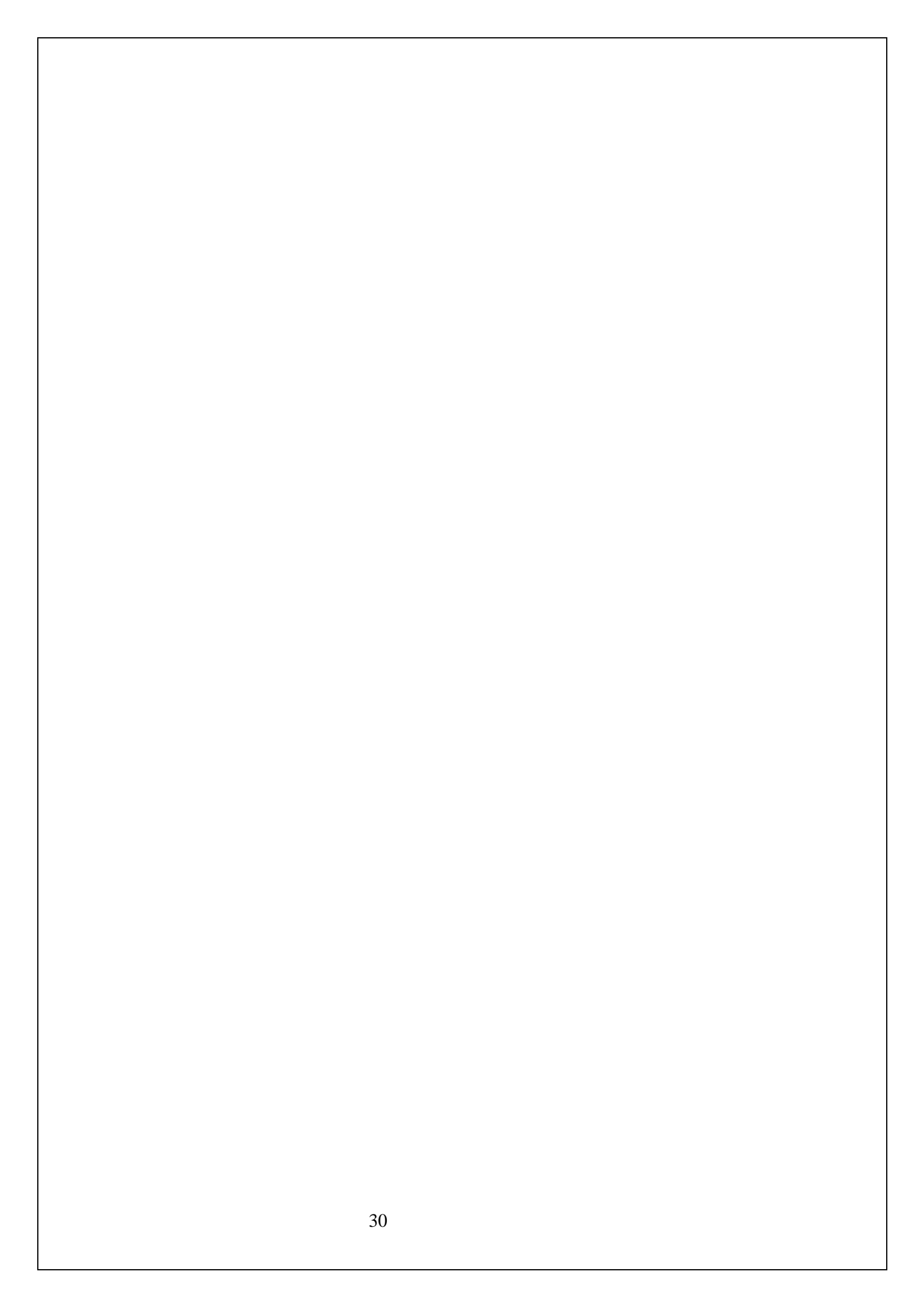
reversibility of the Co-MOF electrode material in the device. This shows that the asymmetric supercapacitor device exhibits fast interfacial charge transfer kinetics and rapid redox reaction dynamics (**Figure 2.4(b)**). Galvanostatic charge-discharge (GCD) measurements were conducted at diverse current densities, demonstrating specific capacitances of 70, 68, 58, 50, 32, and 29.6 F g-1 under varying current densities of 1, 2, 3, 5, 7, and 10 A/g, respectively. The GCD curve exhibits a nearly triangular shape, highlighting the excellent rate capability of the ASC device (**Figure 2.4(c)**). The variation of specific capacitance at different current densities is illustrated in **Figure 2.4(d)**, which supports the observation that there is a decrease in specific capacitance with an increase in current densities, which is due to the fast charge transport occurring at a higher current density.

Notably, the ASC device exhibited a high energy density of 24.88 Wh kg⁻¹ at a corresponding power density of 84.5 W kg⁻¹. In **Figure 2.4(e)**, the Ragone plot demonstrates that the Co-MOF-based ASC device outperforms previously reported cobalt-based MOFs, coordination polymers, and layered frameworks. S67/CC (3.25 W h kg⁻¹ at 275 W kg⁻¹)⁵⁸, Ni–Co–S/NF (24.8W h kg⁻¹ at 849.5 W kg⁻¹)⁵⁹, Co₉S₈/NS (14.85 W h kg⁻¹ at 681.8 W kg⁻¹)⁶⁰, Ni Co-MOF NSHS (20.94 W h kg⁻¹ at 750.84 W kg⁻¹)⁶¹, N-AC/Gr (13.1 W h kg⁻¹ at 12.5 W kg⁻¹)⁶². Furthermore, the device displayed excellent cyclic stability, retaining 87.6% of its initial capacitance after 5000 cycles, underscoring its potential for practical applications (**Figure 2.4(f)**).



CONCLUSIONS

In summary, we have successfully developed a novel cobalt-based functionalized layered framework (Co-MOF) using a mixed-ligand strategy and demonstrated its potential as a high-performance electrode material for supercapacitors. The strategic incorporation of Azopyridine (AzPY) and fluorinated carboxylate (TF) ligands imparts unique structural advantages, including stable hydrogen bonding, π - π interactions, and enhanced electrochemical activity. Co-MOF exhibits superior electrochemical performance, achieving a high specific capacitance of 956 F g⁻¹ at 1A/g with excellent cycling stability and an improved energy density of 24.88 Wh kg⁻¹ in real-time device applications. These findings underscore the significance of ligand structural functionalization and engineering in optimizing electrochemical properties. This work provides valuable insights for the design of advanced electrode materials for next-generation energy storage devices.



SUPPORTING INFORMATION

8.1 Electrode Preparation and Electrochemical Measurement

Carbon cloth (CC) was used as the electrode substrate, with 2 M KOH as the electrolyte, to examine the electrochemical performance of Co-MOF. 1 mg of electrode materials was taken separately and sonicated in 300 μL of ethanolic solution. Then, these samples were drop-cast on CC $(1\times1 \text{ cm}^2)$ and dried at room temperature. The modified electrodes were used for electrochemical studies performed on an Autolab PGSTAT 204N workstation. The assessments were performed at ambient temperature using a conventional three-electrode setup. Specifically, the electrochemical cell consisted of a platinum wire counter electrode, an electrode, carbon cloth Ag/AgCl reference and (CC) working electrode. The electrochemical properties of the synthesized Co-MOF electroactive material were comprehensively evaluated using a trio of key techniques: potentiation cyclic voltammetry (CV), galvanostatic charge-discharge (GCD), and electrochemical impedance spectroscopy (EIS).

8.2 Efficiency Evaluation

The electrochemical performance of Co-MOF was evaluated using galvanostatic charge-discharge (GCD) measurements. The specific capacitance (C_S) was calculated using the following equation:

$$C_S = \frac{I \, \Delta t}{m \Delta V} \tag{1}$$

where I/m is the current density, Δt is the discharge time, and ΔV is the potential range of the GCD profile. The specific capacity (Q) of Co-MOF was estimated using the following equation

$$Q = \frac{I \Delta t}{m} \tag{2}$$

I/m is the current density, and Δt is the discharge time.

8.3 Device Fabrication

We utilized Co-MOF (active material) as the positive electrode, carbon black as the negative electrode, cellulose paper as the separator, carbon paper (2x4 cm) as the substrate, and 1M KOH/PVA as gel electrolyte

for device fabrication. Initially, 5 mg cm⁻² of active material was pasted on carbon paper, and the negative electrode (5 mg cm⁻²) was prepared by mixing activated carbon and PVDF (85:15) and coating it onto another substrate of carbon paper. The device was assembled with a separator between the positive and negative electrodes. It was then charged using a 300 mAh adapter, and the assembled device successfully powered a commercial LED bulb.

The energy density (E) and power density (P) of the asymmetric device (ASC) were determined using the following equations:

$$E = \frac{c_S}{2 \times 3.6} \times \Delta V^2$$

(3)

$$P = \frac{E}{\Delta t} \times 3600$$

(4)

where Cs represents the specific capacitance, ΔV is the potential window, and Δt is the discharge time of the GCD profile.

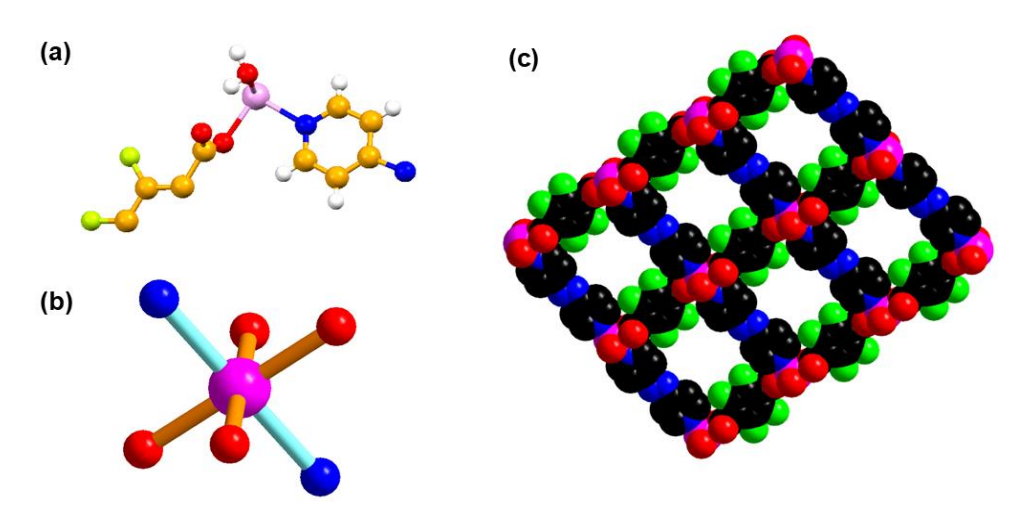


Figure 8.1. SCXRD data of Co-MOF (a) asymmetric unit, (b) metal coordination geometry, (c) Space filling model.

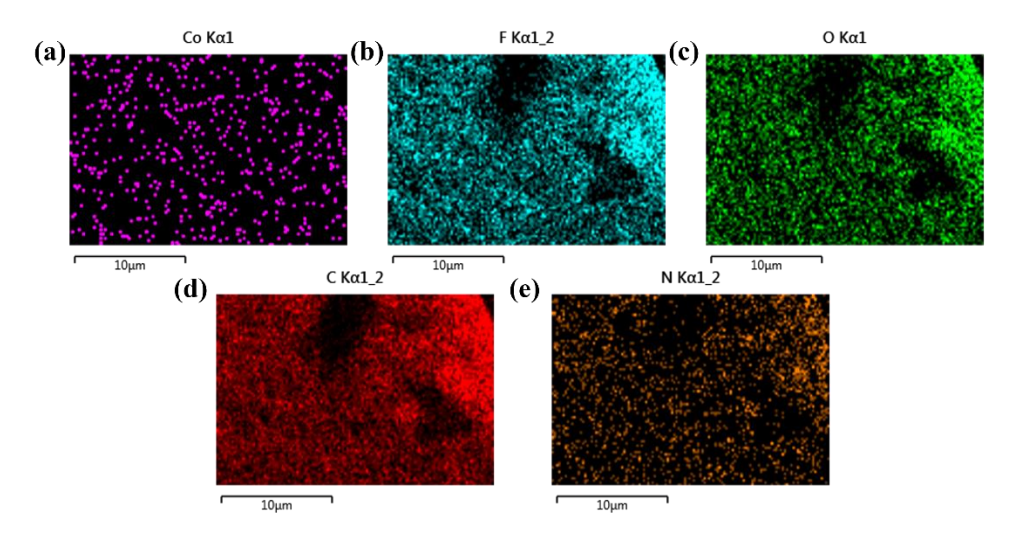


Figure 8.2. EDS Mapping of elements (a) Cobalt, (b) Flourine, (c) Oxygen, (d) Carbon, and (e) Nitrogen

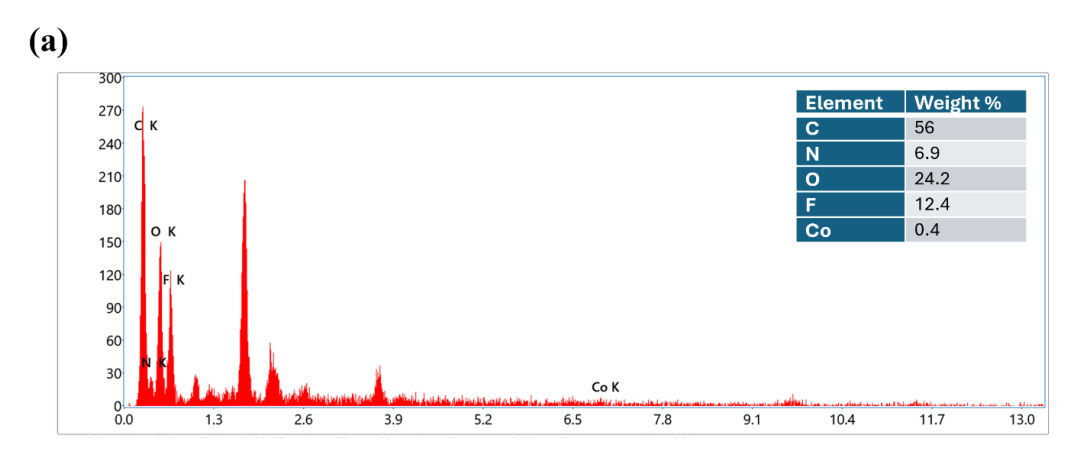


Figure 8.3. (a) EDS elemental analysis Co-MOF (inset: Weight percentage of each element)

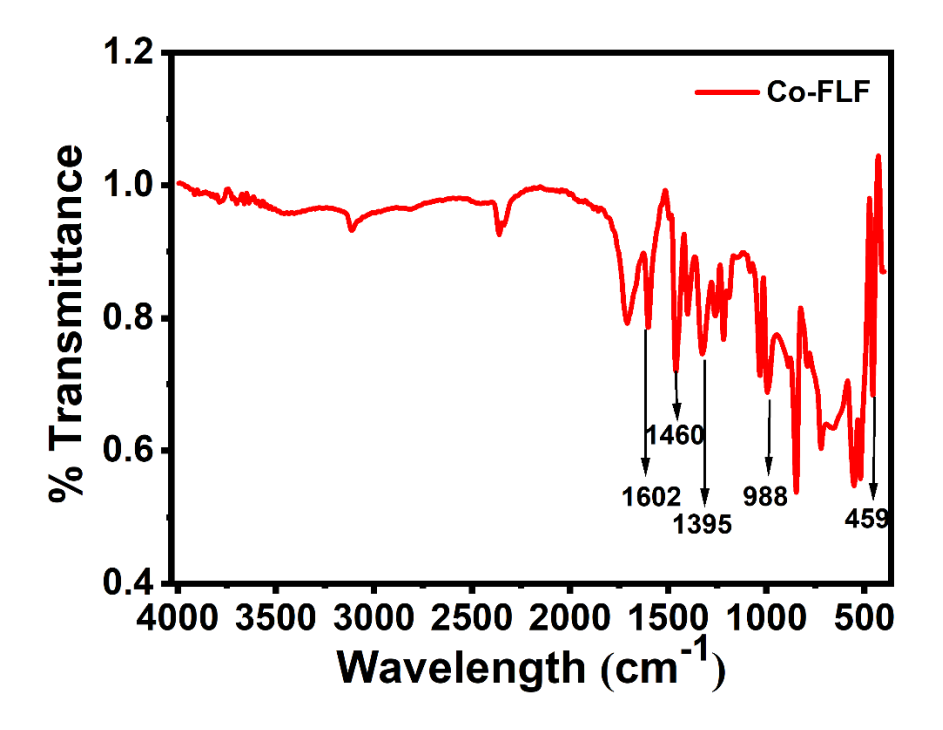


Figure 8.4. FT-IR spectra of Co-MOF.

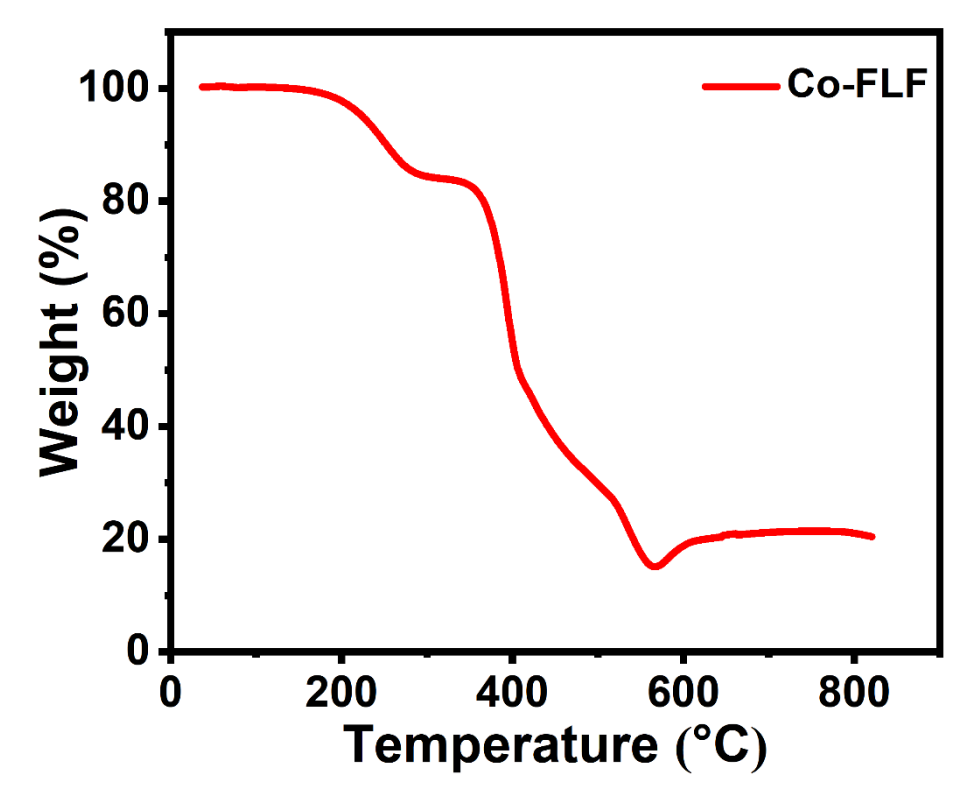


Figure 8.5. Thermogravimetric Profile of Co-MOF.

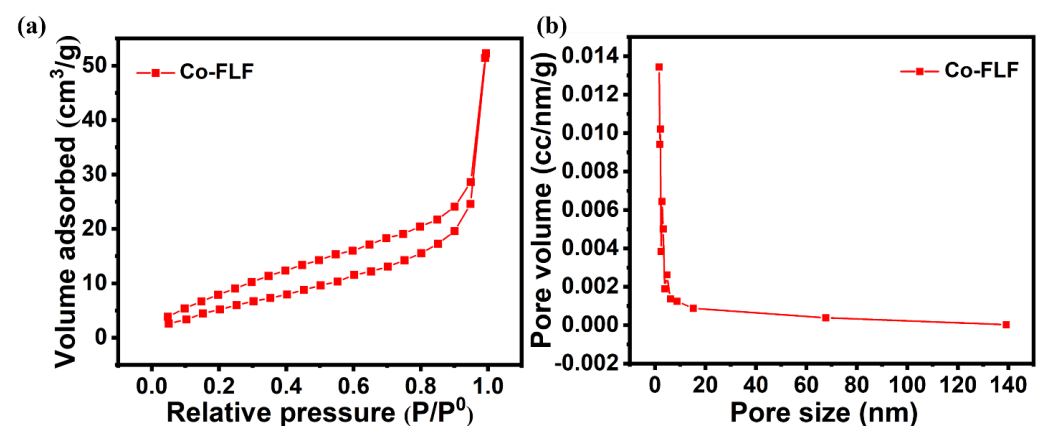


Figure 8.6. (a) BET adsorption-desorption isotherm of Co-MOF (b) BJH distribution of Co-MOF.

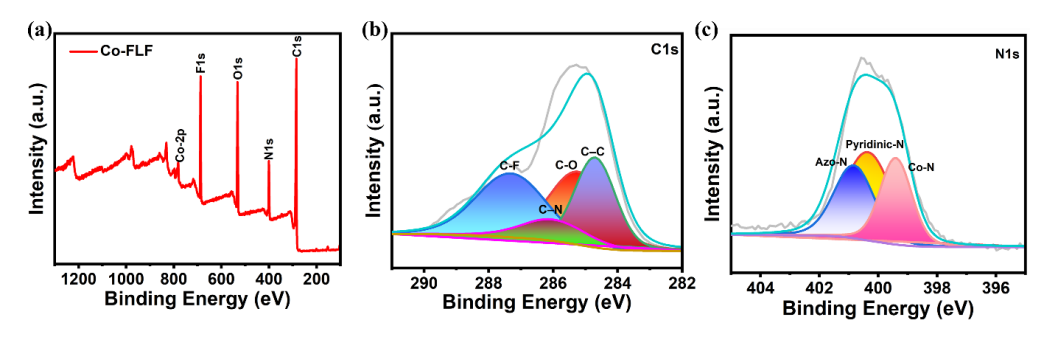


Figure 8.7. XPS spectra of Co-MOF (a) Survey Scan, (b) C 1s and (c) N 1s.

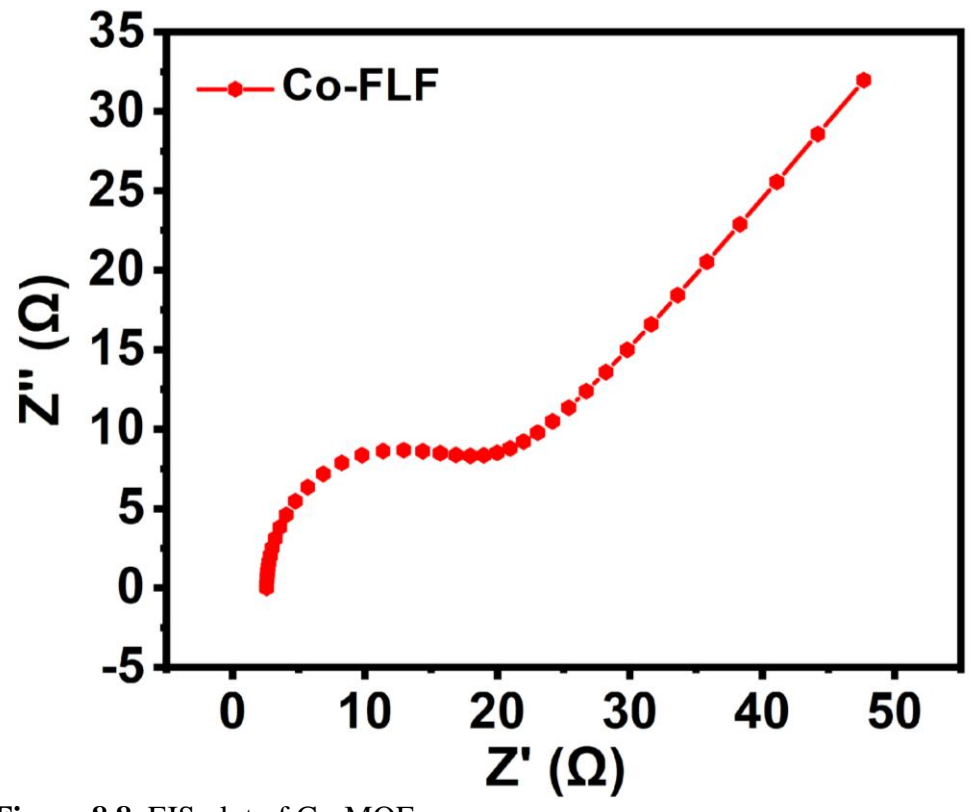


Figure 8.8. EIS plot of Co-MOF.

Table 8.1. X-ray crystal structure data and refinement parameters of Co-MOF.

Identification code	Co-MOF		
Empirical formula	C ₉ H ₆ Co _{0.50} F ₂ N ₂ O ₃		
Formula weight	257.62		
Crystal system	Triclinic		
Space group	P -1		
a (Å)	6.9776(12)		
b (Å)	7.973(3)		
c (Å)	9.575(2)		
α (°)	79.20(3)		
β (°)	70.959(19)		
γ (°)	88.84(2)		
V (Å ³)	494.2(2)		
Z, d _{calcd} (mg m ⁻³)	2, 1.731		
Temperature (K)	293(2)		
Wavelength (Å)	0.71073		
θ range/	3.091 to 28.864		
goodness-of-fit (GOOF)	0.895		
R_1 , a w R_2 b $[I > 2\sigma(I)]$	$R_1 = 0.0816$, $wR_2 = 0.1662$		
R ₁ , a wR ₂ b (all data)	$R_1 = 0.1840, wR_2 = 0.2228$		
absorption correction	Semi-empirical from equivalents		
index ranges	-9<=h<=9, -10<=k<=10, -		
	10<=l<=12		
crystal size (mm ³)	0.360 x 0.280 x 0.230 mm		
refinement method	Full-matrix least-squares on F ²		
Reflections collected / unique	3670 / 2177 [R(int) = 0.1594]		
F (000)	259		

Table 8.2. Bond lengths (Å) and bond angles (°) for Co-MOF

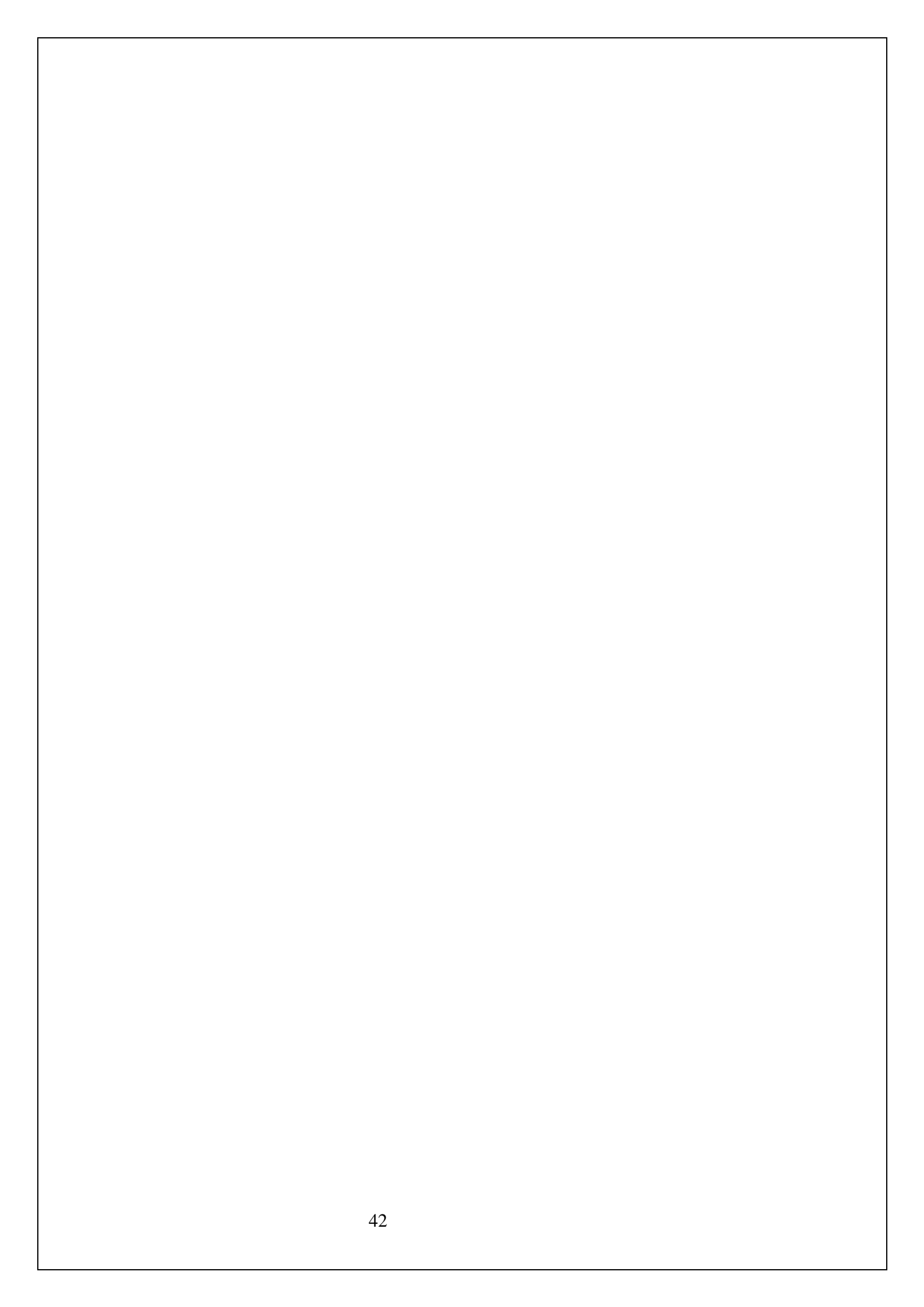
Bond Lengths (Å)				
Co(1)-O(1)#1	2.124(4)			
Co(1)-O(1)	2.124(4)			
Co(1)-O(3)	2.141(4)			
Co(1)-O(3)#1	2.141(4)			
Co(1)-N(1)	2.219(6)			
Co(1)-N(1)#1	2.219(6)			
F(1)-C(3)	1.372(8)			
F(2)-C(4)	1.364(8)			
N(1)-C(5)	1.339(10)			
N(1)-C(9)	1.350(9)			
N(2)-N(2)#2	1.193(13)			
N(2)-C(7)	1.508(10)			
O(1)-C(1)	1.272(6)			
O(2)-C(1)	1.256(8)			
O(3)-H(3A)	0.8504			
O(3)-H(3B)	0.8503			
C(1)-C(2)	1.536(10)			
C(2)-C(3)	1.382(10)			
C(2)-C(4)#3	1.395(10)			
C(3)-C(4)	1.400(11)			
C(5)-C(6)	1.390(10)			
C(5)-H(5)	0.9300			
C(6)-C(7)	1.357(11)			
C(6)-H(6)	0.9300			
C(7)-C(8)	1.373(11)			
C(8)-C(9)	1.421(10)			
C(8)-H(8)	0.9300			
C(9)-H(9)	0.9300			
Bond Angles (°)				
O(1)#1-Co(1)-O(1)	180.0			
O(1)#1-Co(1)-O(3)	88.91(17)			
O(1)-Co(1)-O(3)	91.09(18)			
O(1)#1-Co(1)-O(3)#1	91.09(17)			
O(1)-Co(1)-O(3)#1	88.91(17)			

O(3)-Co(1)-O(3)#1	180.0	
O(1)#1-Co(1)-N(1)	91.7(2)	
O(1)-Co(1)-N(1)	88.3(2)	
O(3)-Co(1)-N(1)	88.17(19)	
O(3)#1-Co(1)-N(1)	91.83(19)	
O(1)#1-Co(1)-N(1)#1	88.3(2)	
O(1)-Co(1)-N(1)#1	91.7(2)	
O(3)-Co(1)-N(1)#1	91.83(19)	
O(3)#1-Co(1)-N(1)#1	88.17(19)	
N(1)-Co(1)-N(1)#1	180.0	
C(5)-N(1)-C(9)	116.7(7)	
C(5)-N(1)-Co(1)	120.1(6)	
C(9)-N(1)-Co(1)	123.1(5)	
N(2)#2-N(2)-C(7)	112.2(10)	
C(1)-O(1)-Co(1)	131.1(5)	
Co(1)-O(3)-H(3A)	109.6	
Co(1)-O(3)-H(3B)	109.1	
H(3A)-O(3)-H(3B)	104.5	
O(2)-C(1)-O(1)	128.9(7)	
O(2)-C(1)-C(2)	117.5(5)	
O(1)-C(1)-C(2)	113.6(6)	
C(3)-C(2)-C(4)#3	116.3(7)	
C(3)-C(2)-C(1)	121.6(7)	
C(4)#3-C(2)-C(1)	122.1(6)	
F(1)-C(3)-C(2)	119.9(7)	
F(1)-C(3)-C(4)	118.2(8)	
C(2)-C(3)-C(4)	121.9(8)	
F(2)-C(4)-C(2)#3	118.7(7)	
F(2)-C(4)-C(3)	119.5(8)	
C(2)#3-C(4)-C(3)	121.8(7)	
N(1)-C(5)-C(6)	124.9(9)	
N(1)-C(5)-H(5)	117.5	
C(6)-C(5)-H(5)	117.5	
C(7)-C(6)-C(5)	117.0(8)	
C(7)-C(6)-H(6)	121.5	
C(5)-C(6)-H(6)	121.5	
C(6)-C(7)-C(8)	121.6(8)	
C(6)-C(7)-N(2)	114.8(7)	

C(8)-C(7)-N(2)	123.6(8)
C(7)-C(8)-C(9)	117.5(8)
C(7)-C(8)-H(8)	121.3
C(9)-C(8)-H(8)	121.3
N(1)-C(9)-C(8)	122.2(8)
N(1)-C(9)-H(9)	118.9
C(8)-C(9)-H(9)	118.9

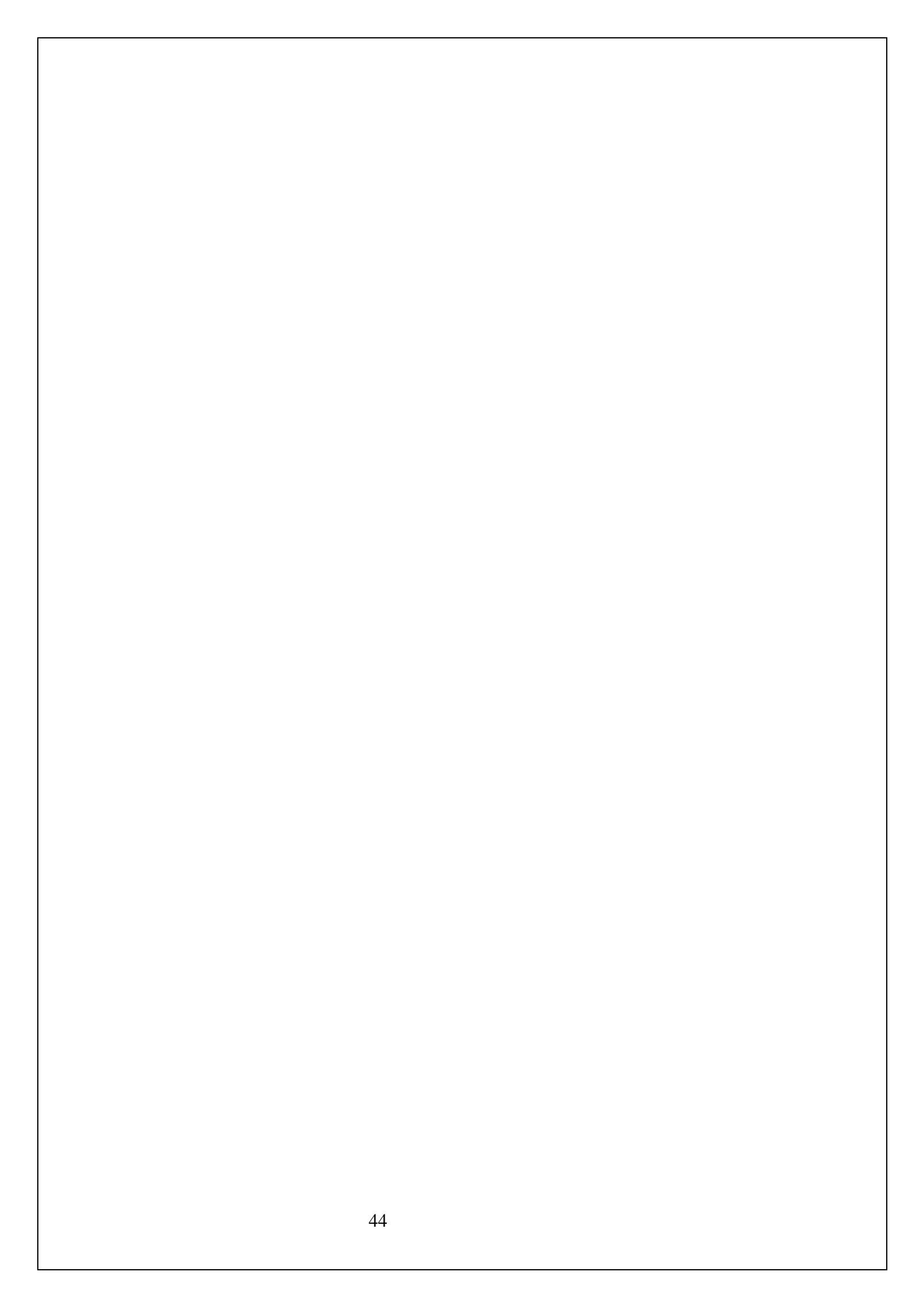
Table 8.3. Supercapacitor performance of Co-MOF compared to other MOF-based materials.

SI.	Active materials	Electrolyte	Specific	Ref
NO			capacitance	
			$(F g^{-1})$	
1	Co-MOF	1 M KOH	446.8	63
2	Co, N-doped CP	6 M KOH	330	64
3	Ni-Co-MOF	3 М КОН	827.9	65
4	Co-MOF derived	2 M KOH	226.1	66
	Co ₃ O ₄			
5	Co-MOF	КОН	469.5	58
	(S67/CC-thiourea)			
6	N-AC/Gr	6 M KOH	378.9	62
7	Co-MOF	6 M KOH	425	67
8	Co-NTA	3 М КОН	395	68
9	NF-FASC	КОН	351.6	69
10	KA@MOF-S	1 M H ₂ SO ₄	648	70
11	Co-MP	3 М КОН	432.6	71
12	Co-MOF	2M KOH	956	THIS
				wo
				RK



SCOPE OF WORK

In this study, we synthesized a novel cobalt-based functionalized layered framework (Co-MOF) using a mixed-ligand strategy via a slow diffusion method and characterized it with single-crystal analysis and other structural analyses. Along with fluorine functionalization, the unique structural architecture of the layered framework, including stable hydrogen bonding and π - π interactions, enhance the electrochemical properties of the Co-MOF. Co-MOF showcasing a superior specific capacitance of (956 F g⁻¹). In addition to the improved electrochemical performance, the Co-MOF also shows a cyclic retention of capacitance of 82%. Furthermore, an asymmetric supercapacitor device was developed using Co-MOF, exhibiting an excellent energy density of 24.88 Wh kg⁻¹. This work provides insightful ideas for the design of new electrode materials for advanced energy storage devices and highlights the advantages of ligand functionalization and structural engineering approaches to optimize electrochemical properties. It contributes important knowledge for the design of advanced electrode materials for next-generation energy storage devices.



REFERENCES

- Kirlikovali, K. O.; Hanna, S. L.; Son, F. A.; Farha, O. K. Back to the Basics: Developing Advanced Metal–Organic Frameworks Using Fundamental Chemistry Concepts. *ACS Nanosci. Au* 2023, 3 (1), 37–45. https://doi.org/10.1021/acsnanoscienceau.2c00046.
- (2) Rangnekar, N.; Mittal, N.; Elyassi, B.; Caro, J.; Tsapatsis, M. Zeolite Membranes a Review and Comparison with MOFs. *Chemical Society Reviews* **2015**, *44* (20), 7128–7154. https://doi.org/10.1039/C5CS00292C.
- (3) Freund, R.; Zaremba, O.; Arnauts, G.; Ameloot, R.; Skorupskii, G.; Dincă, M.; Bavykina, A.; Gascon, J.; Ejsmont, A.; Goscianska, J.; Kalmutzki, M.; Lächelt, U.; Ploetz, E.; Diercks, C. S.; Wuttke, S. The Current Status of MOF and COF Applications. *Angewandte Chemie International Edition* 2021, 60 (45), 23975–24001. https://doi.org/10.1002/anie.202106259.
- (4) Hong, D. H.; Shim, H. S.; Ha, J.; Moon, H. R. MOF-on-MOF Architectures: Applications in Separation, Catalysis, and Sensing. *Bulletin of the Korean Chemical Society* 2021, 42 (7), 956–969. https://doi.org/10.1002/bkcs.12335.
- (5) Kitagawa, S. Future Porous Materials. *Acc. Chem. Res.* 2017, *50*(3), 514–516. https://doi.org/10.1021/acs.accounts.6b00500.
- (6) From fundamentals to applications: a toolbox for robust and multifunctional MOF materials - Chemical Society Reviews (RSC Publishing) DOI:10.1039/C8CS00688A. https://pubs.rsc.org/en/content/articlehtml/2018/cs/c8cs00688a.
- (7) Kleist, W.; Maciejewski, M.; Baiker, A. MOF-5 Based Mixed-Linker Metal–Organic Frameworks: Synthesis, Thermal Stability and Catalytic Application. *Thermochimica Acta* **2010**, *499* (1–2), 71–78. https://doi.org/10.1016/j.tca.2009.11.004.
- (8) Deria, P.; E. Mondloch, J.; Karagiaridi, O.; Bury, W.; T. Hupp, J.; K. Farha, O. Beyond Post-Synthesis Modification: Evolution of Metal-Organic Frameworks via Building Block Replacement.

- *Chemical Society Reviews* **2014**, *43* (16), 5896–5912. https://doi.org/10.1039/C4CS00067F.
- (9) A. Ejegbavwo, O.; A. Berseneva, A.; R. Martin, C.; A. Leith, G.; Pandey, S.; J. Brandt, A.; Chul Park, K.; Mathur, A.; Farzandh, S.; V. Klepov, V.; J. Heiser, B.; Chandrashekhar, M.; G. Karakalos, S.; D. Smith, M.; R. Phillpot, S.; Garashchuk, S.; A. Chen, D.; B. Shustova, N. Heterometallic Multinuclear Nodes Directing MOF Electronic Behavior. *Chemical Science* 2020, *11* (28), 7379–7389. https://doi.org/10.1039/D0SC03053H.
- (10) Cai, M.; Loague, Q.; Morris, A. J. Design Rules for Efficient Charge Transfer in Metal–Organic Framework Films: The Pore Size Effect. *J. Phys. Chem. Lett.* **2020**, *11* (3), 702–709. https://doi.org/10.1021/acs.jpclett.9b03285.
- (11) Stock, N.; Biswas, S. Synthesis of Metal-Organic Frameworks (MOFs): Routes to Various MOF Topologies, Morphologies, and Composites. *Chem. Rev.* 2012, 112 (2), 933–969. https://doi.org/10.1021/cr200304e.
- (12) Głowniak, S.; Szczęśniak, B.; Choma, J.; Jaroniec, M. Advances in Microwave Synthesis of Nanoporous Materials. *Advanced Materials* 2021, 33 (48), 2103477. https://doi.org/10.1002/adma.202103477.
- (13) Szczęśniak, B.; Borysiuk, S.; Choma, J.; Jaroniec, M. Mechanochemical Synthesis of Highly Porous Materials. *Mater. Horiz.* 2020, 7 (6), 1457–1473. https://doi.org/10.1039/D0MH00081G.
- (14) Głowniak, S.; Szczęśniak, B.; Choma, J.; Jaroniec, M. Recent Developments in Sonochemical Synthesis of Nanoporous Materials. *Molecules* 2023, 28 (6), 2639. https://doi.org/10.3390/molecules28062639.
- (15) Oliva González, C. M.; Kharisov, B. I.; Kharissova, O. V.; Serrano Quezada, T. E. Synthesis and Applications of MOF-Derived Nanohybrids: A Review. *Materials Today: Proceedings* 2021, 46, 3018–3029.
 - https://doi.org/10.1016/j.matpr.2020.12.1231.

- (16) Xie, J.; Yang, P.; Wang, Y.; Qi, T.; Lei, Y.; Li, C. M. Puzzles and Confusions in Supercapacitor and Battery: Theory and Solutions. *Journal of Power Sources* **2018**, *401*, 213–223. https://doi.org/10.1016/j.jpowsour.2018.08.090.
- (17) Raza, W.; Ali, F.; Raza, N.; Luo, Y.; Kim, K.-H.; Yang, J.; Kumar, S.; Mehmood, A.; Kwon, E. E. Recent Advancements in Supercapacitor Technology. *Nano Energy* **2018**, *52*, 441–473. https://doi.org/10.1016/j.nanoen.2018.08.013.
- (18) Peng, Y.; Xu, J.; Xu, J.; Ma, J.; Bai, Y.; Cao, S.; Zhang, S.; Pang, H. Metal-Organic Framework (MOF) Composites as Promising Materials for Energy Storage Applications. *Advances in Colloid and Interface Science* 2022, 307, 102732. https://doi.org/10.1016/j.cis.2022.102732.
- (19) Peng, J.; Zhao, Y.; Wang, X.; Zeng, X.; Wang, J.; Hou, S. Metal-Organic Frameworks: Advances in First-Principles Computational Studies on Catalysis, Adsorption, and Energy Storage. *Materials Today Communications* 2024, 40, 109780. https://doi.org/10.1016/j.mtcomm.2024.109780.
- (20) Baumann, A. E.; Burns, D. A.; Liu, B.; Thoi, V. S. Metal-Organic Framework Functionalization and Design Strategies for Advanced Electrochemical Energy Storage Devices. *Commun Chem* 2019, 2 (1), 86. https://doi.org/10.1038/s42004-019-0184-6.
- (21) He, B.; Zhang, Q.; Pan, Z.; Li, L.; Li, C.; Ling, Y.; Wang, Z.; Chen, M.; Wang, Z.; Yao, Y.; Li, Q.; Sun, L.; Wang, J.; Wei, L. Freestanding Metal—Organic Frameworks and Their Derivatives: An Emerging Platform for Electrochemical Energy Storage and Conversion. *Chem. Rev.* **2022**, *122* (11), 10087–10125. https://doi.org/10.1021/acs.chemrev.1c00978.
- (22) Shahbazi Farahani, F.; Rahmanifar, M. S.; Noori, A.; El-Kady, M. F.; Hassani, N.; Neek-Amal, M.; Kaner, R. B.; Mousavi, M. F. Trilayer Metal—Organic Frameworks as Multifunctional Electrocatalysts for Energy Conversion and Storage Applications.

- *J. Am. Chem. Soc.* **2022**, *144* (8), 3411–3428. https://doi.org/10.1021/jacs.1c10963.
- (23) Wang, L.; Feng, X.; Ren, L.; Piao, Q.; Zhong, J.; Wang, Y.; Li, H.; Chen, Y.; Wang, B. Flexible Solid-State Supercapacitor Based on a Metal–Organic Framework Interwoven by Electrochemically-Deposited PANI. *J. Am. Chem. Soc.* 2015, 137 (15), 4920–4923. https://doi.org/10.1021/jacs.5b01613.
- (24) Wang, W.; Zhang, L.; Xu, G.; Song, H.; Yang, L.; Zhang, C.; Xu, J.; Jia, D. Structure-Designed Synthesis of CoP Microcubes from Metal–Organic Frameworks with Enhanced Supercapacitor Properties. *Inorg. Chem.* 2018, 57 (16), 10287–10294. https://doi.org/10.1021/acs.inorgchem.8b01524.
- (25) Khan, J.; Iqbal, M. Z.; Rubab, B.; Jamshaid, F.; Khan, A.; Shakeel, N.; Ahmed, A.; Al-Kahtani, A. A. Isonicotinic Acid-Based Copper-MOF: An Exotic Redox Propertied Electrode Material for High Energy Asymmetric Supercapacitor. *Journal of Energy Storage* 2023, 72, 108655. https://doi.org/10.1016/j.est.2023.108655.
- (26) Hou, X.; Sun, J.; Lian, M.; Peng, Y.; Jiang, D.; Xu, M.; Li, B.; Xu, Q. Emerging Synthetic Methods and Applications of MOF-Based Gels in Supercapacitors, Water Treatment, Catalysis, Adsorption, and Energy Storage. *Macromolecular Materials and Engineering* 2023, 308 (2), 2200469. https://doi.org/10.1002/mame.202200469.
- (27) Dar, M. A.; Majid, S. R.; Satgunam, M.; Siva, C.; Ansari, S.; Arularasan, P.; Rafi Ahamed, S. Advancements in Supercapacitor Electrodes and Perspectives for Future Energy Storage Technologies. *International Journal of Hydrogen Energy* **2024**, 70, 10–28. https://doi.org/10.1016/j.ijhydene.2024.05.191.
- (28) Kandasamy, M.; Sahoo, S.; Nayak, S. K.; Chakraborty, B.; Rout, C. S. Recent Advances in Engineered Metal Oxide Nanostructures for Supercapacitor Applications: Experimental and Theoretical Aspects. *J. Mater. Chem. A* 2021, 9 (33), 17643–17700. https://doi.org/10.1039/D1TA03857E.

- (29) Wang, Q.; Astruc, D. State of the Art and Prospects in Metal–Organic Framework (MOF)-Based and MOF-Derived Nanocatalysis. *Chem. Rev.* **2020**, *120* (2), 1438–1511. https://doi.org/10.1021/acs.chemrev.9b00223.
- (30) Freund, R.; Zaremba, O.; Arnauts, G.; Ameloot, R.; Skorupskii, G.; Dincă, M.; Bavykina, A.; Gascon, J.; Ejsmont, A.; Goscianska, J.; Kalmutzki, M.; Lächelt, U.; Ploetz, E.; Diercks, C. S.; Wuttke, S. The Current Status of MOF and COF Applications. *Angewandte Chemie International Edition* 2021, 60 (45), 23975–24001. https://doi.org/10.1002/anie.202106259.
- (31) Liu, J.; Song, X.; Zhang, T.; Liu, S.; Wen, H.; Chen, L. 2D Conductive Metal–Organic Frameworks: An Emerging Platform for Electrochemical Energy Storage. *Angewandte Chemie* **2021**, *133* (11), 5672–5684. https://doi.org/10.1002/ange.202006102.
- (32) Wu, H.; Zhang, W.; Kandambeth, S.; Shekhah, O.; Eddaoudi, M.; Alshareef, H. N. Conductive Metal–Organic Frameworks Selectively Grown on Laser-Scribed Graphene for Electrochemical Microsupercapacitors. *Advanced Energy Materials* 2019, 9 (21), 1900482. https://doi.org/10.1002/aenm.201900482.
- (33) Gupta, A. K.; Saraf, M.; Bharadwaj, P. K.; Mobin, S. M. Dual Functionalized CuMOF-Based Composite for High-Performance Supercapacitors. *Inorg. Chem.* **2019**, *58* (15), 9844–9854. https://doi.org/10.1021/acs.inorgchem.9b00909.
- (34) Zhang, X.; Liu, X.; Zeng, Y.; Tong, Y.; Lu, X. Oxygen Defects in Promoting the Electrochemical Performance of Metal Oxides for Supercapacitors: Recent Advances and Challenges. *Small Methods* 2020, 4 (6), 1900823. https://doi.org/10.1002/smtd.201900823.
- (35) Ye, W.; Wang, H.; Shen, J.; Khan, S.; Zhong, Y.; Ning, J.; Hu, Y. Halogen-Based Functionalized Chemistry Engineering for High-Performance Supercapacitors. *Chinese Chemical Letters* **2023**, *34* (1), 107198. https://doi.org/10.1016/j.cclet.2022.02.004.

- (36) Zhu, T.; Liu, S.; Wan, K.; Zhang, C.; Feng, Y.; Feng, W.; Liu, T. Fluorine and Nitrogen Dual-Doped Porous Carbon Nanosheet-Enabled Compact Electrode Structure for High Volumetric Energy Storage. *ACS Appl. Energy Mater.* **2020**, *3* (5), 4949–4957. https://doi.org/10.1021/acsaem.0c00500.
- (37) Zhao, Y.; Huang, C.; He, Y.; Wu, X.; Ge, R.; Zu, X.; Li, S.; Qiao, L. High-Performance Asymmetric Supercapacitors Realized by Copper Cobalt Sulfide Crumpled Nanoflower and N, F Co-Doped Hierarchical Nanoporous Carbon Polyhedron. *Journal of Power Sources* 2020, 456, 228023. https://doi.org/10.1016/j.jpowsour.2020.228023.
- (38) Chu, S.; Majumdar, A. Opportunities and Challenges for a Sustainable Energy Future. *Nature* **2012**, *4*88 (7411), 294–303. https://doi.org/10.1038/nature11475.
- (39) Chen, N.; Huang, X.; Qu, L. Heteroatom Substituted and Decorated Graphene: Preparation and Applications. *Phys. Chem. Chem. Phys.* **2015**, *17* (48), 32077–32098. https://doi.org/10.1039/C5CP04391C.
- (40) Ma, T.; Liu, X.; Wang, X.; Ma, J.-G.; Cheng, P. Bottom-Up Construction of Rhombic Lamellar CoNi-MOFs for the Electrochemical Sensing of H2S. *Inorg. Chem.* **2024**, *63* (16), 7504–7511. https://doi.org/10.1021/acs.inorgchem.4c00862.
- (41) Sheldrick, G. M. A Short History of SHELX. *Acta Cryst A* **2008**, *64* (1), 112–122. https://doi.org/10.1107/S0108767307043930.
- (42) Bergerhoff, G.; Berndt, M.; Brandenburg, K. Evaluation of Crystallographic Data with the Program DIAMOND. *J Res Natl Inst Stand Technol* 1996, 101 (3), 221–225. https://doi.org/10.6028/jres.101.023.
- (43) Hu, X.; Hu, H.; Li, C.; Li, T.; Lou, X.; Chen, Q.; Hu, B. Cobalt-Based Metal Organic Framework with Superior Lithium Anodic Performance. *Journal of Solid State Chemistry* **2016**, 242, 71–76. https://doi.org/10.1016/j.jssc.2016.07.021.
- (44) Hu, X.; Hu, H.; Li, C.; Li, T.; Lou, X.; Chen, Q.; Hu, B. Cobalt-Based Metal Organic Framework with Superior Lithium Anodic

- Performance. *Journal of Solid State Chemistry* **2016**, 242, 71–76. https://doi.org/10.1016/j.jssc.2016.07.021.
- (45) Karuppasamy, K.; Bose, R.; Vikraman, D.; Ramesh, S.; Kim, H. S.; Alhseinat, E.; Alfantazi, A.; Kim, H.-S. Revealing the Effect of Various Organic Ligands on the OER Activity of MOF-Derived 3D Hierarchical Cobalt Oxide @ Carbon Nanostructures. *Journal of Alloys and Compounds* 2023, 934, 167909. https://doi.org/10.1016/j.jallcom.2022.167909.
- (46) Li, X.; Zhang, H.; Liu, C.; Qiao, J.; Zhou, X. A MOF-Derived Multifunctional Nano-Porous Fluorinated Carbon for High Performance Lithium/Fluorinated Carbon Primary Batteries. *Microporous and Mesoporous Materials* 2021, 310, 110650. https://doi.org/10.1016/j.micromeso.2020.110650.
- (47) Li, Y.; Han, W.; Wang, R.; Weng, L.-T.; Serrano-Lotina, A.; Bañares, M. A.; Wang, Q.; Yeung, K. L. Performance of an Aliovalent-Substituted CoCeOx Catalyst from Bimetallic MOF for VOC Oxidation in Air. *Applied Catalysis B: Environmental* **2020**, 275, 119121. https://doi.org/10.1016/j.apcatb.2020.119121.
- (48) Gu, X.; Ji, Y.-G.; Tian, J.; Wu, X.; Feng, L. Combined MOF Derivation and Fluorination Imparted Efficient Synergism of Fe-Co Fluoride for Oxygen Evolution Reaction. *Chemical Engineering Journal* 2022, 427, 131576. https://doi.org/10.1016/j.cej.2021.131576.
- (49) Xie, Y.; Fan, L.; Liu, W.; Zhang, Q.; Huang, G. Synthesis of Mn/Co-MOF for Effective Removal of U(VI) from Aqueous Solution. *Particuology* 2023, 72, 134–144. https://doi.org/10.1016/j.partic.2022.03.004.
- (50) Han, X.; Chen, W.-M.; Han, X.; Tan, Y.-Z.; Sun, D. Nitrogen-Rich MOF Derived Porous Co3O4/N–C Composites with Superior Performance in Lithium-Ion Batteries. *J. Mater. Chem. A* 2016, 4 (34), 13040–13045. https://doi.org/10.1039/C6TA05096D.
- (51) Zhang, G.; Colin, M.; Yang, X.; Sun, S.; Dodelet, J.-P.; Dubois,M. CF Bonding in Fluorinated N-Doped Carbons. *Applied*

- Surface Science **2022**, 577, 151721. https://doi.org/10.1016/j.apsusc.2021.151721.
- (52) Dou, Y.; Zhou, J.; Yang, F.; Zhao, M.-J.; Nie, Z.; Li, J.-R. Hierarchically Structured Layered-Double-Hydroxide@zeolitic-Imidazolate-Framework Derivatives for High-Performance Electrochemical Energy Storage. *J. Mater. Chem. A* 2016, 4 (32), 12526–12534. https://doi.org/10.1039/C6TA04765C.
- (53) Guo, Y.; Wei, Y.; Li, H.; Zhai, T. Layer Structured Materials for Advanced Energy Storage and Conversion. *Small* **2017**, *13* (45), 1701649. https://doi.org/10.1002/smll.201701649.
- (54) Schneemann, A.; Dong, R.; Schwotzer, F.; Zhong, H.; Senkovska, I.; Feng, X.; Kaskel, S. 2D Framework Materials for Energy Applications. *Chem. Sci.* 2021, 12 (5), 1600–1619. https://doi.org/10.1039/D0SC05889K.
- (55) Ye, W.; Wang, H.; Shen, J.; Khan, S.; Zhong, Y.; Ning, J.; Hu, Y. Halogen-Based Functionalized Chemistry Engineering for High-Performance Supercapacitors. *Chinese Chemical Letters* 2023, 34 (1), 107198. https://doi.org/10.1016/j.cclet.2022.02.004.
- (56) Gao, Y.; Zhi, C.; Cui, P.; Zhang, K. A. I.; Lv, L.-P.; Wang, Y. Halogen-Functionalized Triazine-Based Organic Frameworks towards High Performance Supercapacitors. *Chemical Engineering Journal* 2020, 400, 125967. https://doi.org/10.1016/j.cej.2020.125967.
- (57) Pal, A.; Ghosh, S.; Singha, D.; Nandi, M. Morphology Controlled Synthesis of Heteroatom-Doped Spherical Porous Carbon Particles Retaining High Specific Capacitance at High Current Density. ACS Appl. Energy Mater. 2021, 4 (10), 10810–10825. https://doi.org/10.1021/acsaem.1c01786.
- (58) Xiao, C.-Y.; Chen, T.-Y.; Chung, R.-J.; Yougbaré, S.; Lin, L.-Y.; Wu, Y.-F. Binder-Free Synthesis of Metal Organic Framework Derived Cobalt Sulfide on Carbon Cloth for Efficient Energy Storage Devices. *Journal of Energy Storage* 2022, 55, 105622. https://doi.org/10.1016/j.est.2022.105622.

- (59) Tao, K.; Han, X.; Ma, Q.; Han, L. A Metal–Organic Framework Derived Hierarchical Nickel–Cobalt Sulfide Nanosheet Array on Ni Foam with Enhanced Electrochemical Performance for Supercapacitors. *Dalton Trans.* 2018, 47 (10), 3496–3502. https://doi.org/10.1039/C7DT04942K.
- (60) Zhang, S.; Li, D.; Chen, S.; Yang, X.; Zhao, X.; Zhao, Q.; Komarneni, S.; Yang, D. Highly Stable Supercapacitors with MOF-Derived Co₉ S₈ /Carbon Electrodes for High Rate Electrochemical Energy Storage. *J. Mater. Chem. A* 2017, 5 (24), 12453–12461. https://doi.org/10.1039/C7TA03070C.
- (61) Sun, J.; Yu, X.; Zhao, S.; Chen, H.; Tao, K.; Han, L. Solvent-Controlled Morphology of Amino-Functionalized Bimetal Metal-Organic Frameworks for Asymmetric Supercapacitors. *Inorg. Chem.* 2020, *59* (16), 11385–11395. https://doi.org/10.1021/acs.inorgchem.0c01157.
- (62) Xie, Q.; Bao, R.; Zheng, A.; Zhang, Y.; Wu, S.; Xie, C.; Zhao, P. Sustainable Low-Cost Green Electrodes with High Volumetric Capacitance for Aqueous Symmetric Supercapacitors with High Energy Density. ACS Sustainable Chem. Eng. 2016, 4 (3), 1422–1430. https://doi.org/10.1021/acssuschemeng.5b01417.
- (63) Rajak, R.; Saraf, M.; Mohammad, A.; Mobin, S. M. Design and Construction of a Ferrocene Based Inclined Polycatenated Co-MOF for Supercapacitor and Dye Adsorption Applications. *J. Mater. Chem. A* **2017**, *5* (34), 17998–18011. https://doi.org/10.1039/C7TA03773B.
- (64) Díaz-Duran, A. K.; Montiel, G.; Viva, F. A.; Roncaroli, F. Co,N-Doped Mesoporous Carbons Cobalt Derived from Coordination Polymer as Supercapacitors. *Electrochimica Acta* 2019, 299, 987–998. https://doi.org/10.1016/j.electacta.2019.01.023.
- (65) Lee, D. Y.; Yoon, S. J.; Shrestha, N. K.; Lee, S.-H.; Ahn, H.; Han, S.-H. Unusual Energy Storage and Charge Retention in Co-Based Metal–Organic-Frameworks. *Microporous and Mesoporous Materials* 2012, *153*, 163–165. https://doi.org/10.1016/j.micromeso.2011.12.040.

- (66) Tao, Y.; Wu, Y.; Chen, H.; Chen, W.; Wang, J.; Tong, Y.; Pei, G.; Shen, Z.; Guan, C. Synthesis of Amorphous Hydroxyl-Rich Co3O4 for Flexible High-Rate Supercapacitor. *Chemical Engineering Journal* 2020, 396, 125364. https://doi.org/10.1016/j.cej.2020.125364.
- (67) Khan, S.; Halder, S.; Chand, S.; Pradhan, A. K.; Chakraborty, C. Co-Containing Metal—Organic Framework for High-Performance Asymmetric Supercapacitors with Functionalized Reduced Graphene Oxide. *Dalton Trans.* 2023, 52 (40), 14663–14675. https://doi.org/10.1039/D3DT02314A.
- (68) Yan, Y.; Gu, P.; Zheng, S.; Zheng, M.; Pang, H.; Xue, H. Facile Synthesis of an Accordion-like Ni-MOF Superstructure for High-Performance Flexible Supercapacitors. *J. Mater. Chem. A* 2016, 4 (48), 19078–19085. https://doi.org/10.1039/C6TA08331E.
- (69) Liu, Y.; Li, X.; Gao, M.; Hao, X.; Li, J.; Liu, Y.; Li, Y.; Cai, K. High-Energy-Density Asymmetric Supercapacitor Based on a Nickel Cobalt Double Hydroxide/Reduced-Graphene-Oxide Fiber Electrode. ACS Appl. Energy Mater. 2022, 5 (8), 9605–9615. https://doi.org/10.1021/acsaem.2c01243.
- (70) Somnath; Waris; Ali, A.; Ahmad, M.; Siddiqui, K. A. Bifunctional Self-Penetrating Co(II)-Based 3D MOF for High-Performance Environmental and Energy Storage Applications. *Crystal Growth & Design* 2022, 22 (12), 7374–7394. https://doi.org/10.1021/acs.cgd.2c00978.
- (71) Athira, A. R.; Raj, B. N. B.; Xavier, T. S. Microwave-Induced Polyindole on Cobalt MOF-Electrodes for High-Performance Supercapacitors. *J. Electrochem. Soc.* **2021**, *168* (12), 120524. https://doi.org/10.1149/1945-7111/ac3e4c.